Title
Front and Back Instability of a Liquid Film on a Slightly Inclined Plate

Journal
Physics of Fluids, 15

Authors
Thiele, Uwe
Knobloch, Edgar

Publication Date
2003

Peer reviewed

Published in Phys. Fluids 15, 892–907 (2003)

Front and back instability of a liquid film on a slightly inclined plate

Uwe Thiele and Edgar Knobloch

Department of Physics, University of California, Berkeley CA 94720

Abstract

We study the transverse instability of a liquid ridge on horizontal and inclined substrates using a film evolution equation based on a long wave approximation. The equation incorporates an additional pressure term – the disjoining pressure – accounting for the effective interaction of the film with the substrate. On a horizontal substrate the dominant instability mode is varicose, but may turn into a zigzag mode on a slightly inclined substrate depending on the inclination angle and the ridge volume. For larger angles or volumes the instabilities at the front and back decouple. The linear stability properties of a one-dimensional ridge-like state are studied in detail, and an energy analysis is used to demonstrate that the disjoining pressure provides the dominant instability mechanism at both the front and the back, while the body force is responsible for the main differences between these two instabilities. An amplitude equation for the time evolution of perturbations with small transverse wavenumbers is derived that predicts correctly the linear crossing of the most dangerous eigenvalues at zero wavenumber in the inclined case, in contrast to the situation on a horizontal substrate.

Keywords: Thin films, Interfacial instabilities, Instabilities/fingering of interfacial flows, Stability/dynamics of thin films

I. INTRODUCTION

When a fluid sheet flows down an inclined plane the leading front may be unstable to slight perturbations that initiate a fingering instability that develops into an array of straight or wedge-shaped fingers advancing faster than the original front[1]. This instability has been the subject of numerous investigations[2–13]. Linear stability analysis shows that the front is unstable for a band of wavenumbers between zero and a finite limiting value, and that the dispersion relation has a maximum at a finite wavenumber[5]. This qualitative result is independent of the details of the model used for the contact line motion, i.e., of the model of the contact line slip at the substrate, and remains valid if a precursor film is assumed to be present instead. Hydrostatic pressure tends to stabilize the film, and is responsible for the existence of a threshold inclination angle for the onset of the instability[7].

Related transverse (or spanwise) instabilities occur on a liquid front that advances as a result of a Marangoni flow induced by a longitudinal (i.e., streamwise) temperature gradient[14–18], and on a spreading drop of surfactant on a prewetted plane[19–23]. In all three cases a capillary ridge forms at the advancing front, and the general belief is that the observed instabilities are due to differences in the mobility of the thinner and thicker parts of this ridge. Since this ridge tends to be suppressed by hydrostatic pressure the inclusion of this pressure stabilizes the advancing front with respect to transverse perturbations in this case also. However, no studies exist of the corresponding phenomena at a receding front under the influence of a body force. This may be due to the general assumption that such fronts are stable because they are not associated with the presence of a capillary ridge.

In addition to the studies of individual advancing fronts mentioned above HOCKING and MIKSIS studied transverse liquid ridges, i.e., liquid sheets of finite streamwise width, sliding down an inclined plane[24,25] using a slip contact line model with a linear dependence of the dynamic contact angles on the velocity of the contact lines. In models of this type perturbations with a nonzero transverse wavenumber lead to transverse instabilities that involve both the advancing *and* the receding contact lines[25]. When the ridge is assumed to be quasi-stationary linear theory predicts that the largest growth rate occurs for perturbations with vanishing wavenumber (i.e., perturbations on the scale of the system size)[24,25] but once the quasi-stationarity assumption is relaxed the fastest growth occurs at a finite wavenumber[25]. When such a ridge loses stability instability is observed at both the front and the back of the ridge

simultaneously. Inspection of the figures in Ref. 25 shows that the instabilities are coupled and correspond to an asymmetric varicose mode, i.e., where the front bulges forwards the back bulges backwards but to a lesser degree.

It is of interest to note that in contrast to a semi-infinite liquid sheet on a a horizontal substrate a liquid ridge on such a substrate *is* unstable to transverse perturbations[26–28]. In particular, for ridges of small height with negligible gravitational effects DAVIS[26] calculated sufficient stability conditions for ridges with (i) fixed contact lines, (ii) fixed contact angles, and (iii) contact angles that vary smoothly with contact line speed, allowing for slip at the substrate in cases (ii,iii), using an energy-like integral form of the linearized hydrodynamic equations. Refs. 27 and 28 employ similar assumptions but consider more general geometries as well. Both articles examine the second variation of an energy functional to predict the minimum wavelength for the transverse instability, but the former is restricted to small contact angles. Liquid ridges are found to be always transversely unstable but the instability becomes weaker and weaker as the ridge becomes larger and larger. The unstable eigenmode is a varicose mode that extends thicker regions at the expense of thinner ones[27], much as the Rayleigh instability in a liquid jet[29,30]. The varicose mode and the first stable mode – the zigzag mode – are intrinsically related to the neutral modes corresponding to the continuous symmetries of the one-dimensional problem, namely, the invariance with respect to change in liquid volume and invariance under translations in the longitudinal direction.

A general difficulty arising in all problems involving moving contact lines such as spreading drops or liquid sheets or ridges on an inclined plate is that the classical no-slip boundary condition at the liquid-solid interface has to be relaxed to permit movement of the contact line. This can be done by introducing a very thin precursor film, or by allowing for slip near the contact line, or introducing an effective molecular interaction between the substrate and liquid into the hydrodynamic model[31–35]. With the exception of Refs. 10,13 all of the work cited above on moving liquid sheets and ridges uses one of the first two options. Both prescriptions avoid divergence problems at the contact line, but at the expense of introducing ad hoc parameters into the theory. These parameters, namely the slip length or the precursor film thickness, influence the base state profile and hence the growth rate and wavenumber of the fastest growing transverse instability[5,7,15,25]. Moreover, the equilibrium and dynamic contact angles have to be fixed independently when introducing the slip condition[24,33,36]. In contrast, in the absence

of motion the precursor film models require that the contact angle be zero, although once the film is in motion the dynamic contact angle depends on the velocity of the advancing front. In an alternative approach[37] either the vapor-liquid or fluid-solid interface, or both, are treated as separate phases with properties that differ from the bulk fluid.

The third, and most realistic, option is the explicit introduction of molecular interactions into the hydrodynamic formalism. This is accomplished by means of an additional pressure term, the disjoining pressure[38]. Depending on the particular problem treated, this disjoining pressure may incorporate long-range van der Waals and/or various types of short-range interaction terms[39–42]. These interactions are essential for the process of dewetting, and studies of dewetting of a thin liquid film on a substrate are generally based on models involving a disjoining pressure[43–48]. However, only a few studies of instabilities of an advancing liquid front have adopted a similar approach[10,13], despite the fact that such an approach *predicts* all the ad hoc parameters of the slip or precursor models (i.e., the static and dynamic contact angle, drop velocity, and the drop and precursor film thickness) connected with the wetting properties of the liquid in terms of the parameters characterizing the disjoining pressure.

Recently PISMEN and POMEAU[49] derived a film thickness equation with a disjoining pressure term that remains finite even for vanishing film thickness by combining the long wave approximation for thin films[50] with a diffuse interface description for the liquid-gas interface[51]. These authors take into account the deviation of the liquid density from its bulk value in the vicinity of the liquid-solid and liquid-gas interface and discuss the resulting vertical density profile for a horizontal liquid layer on a solid substrate. The sharp liquid-gas interface is thereby replaced by a smooth transition between liquid and gas densities. Likewise, the density varies close to the solid substrate due to molecular interactions that enter into the calculation via the boundary condition for the fluid density at the substrate. The resulting density profile is then incorporated into a fully consistent theory based on the Stokes equation in the long wave approximation to take into account dynamical situations. The film thickness equation that results has the usual form of a thin film equation with a disjoining pressure[50], but the disjoining pressure is purely hydrodynamic in origin and its form is derived self-consistently rather than modeled. For reasons already discussed this equation admits instabilities of the homogeneous (i.e., flat) film, and the resulting structure formation was investigated both for a liquid film on a horizontal substrate[48,52] and for a film flowing down a slightly inclined plane[53]. Very recent

two-dimensional simulations of sliding drops and liquid ridges on an inclined plane using this model[13,54] revealed the presence of transverse instabilities at both the front and the back of the ridge, apparently with different wavenumbers even in the linear regime of the instability. Related simulations of sliding drops have revealed a sequence of transitions in the drop shape with increasing inclination angle, from an elongated drop to one with a cusp at the upstream tip, and then to a drop with a cusp that emits small satellite droplets much as observed experimentally[55].

Motivated by these and other results on advancing fronts and ridges, we study here the linear stability of liquid ridges on horizontal and inclined substrates as a function of their volume and the inclination angle of the substrate. For inclined substrates we take the ridge to be transverse, i.e., perpendicular to the slope. Our aim is on the one hand to understand the transition between the varicose instability present on a horizontal substrate and the asymmetric varicose or zigzag instabilities of ridges on an inclined plane, and on the other hand to relate these findings to existing results for a falling semi-infinite sheet obtained with different microscopic models. In other words, we are interested in understanding the role played by the back instability found in Ref. 54, and its coupling to the better known instability at the front.

Our study is organized as follows. In Section II we introduce the evolution equation for the film thickness, discuss the form of the disjoining pressure used, and nondimensionalize the equations. In Section III we discuss the strategy used to determine stationary solutions and their linear stability properties. Section IV gives the results for the transverse stability of a ridge on horizontal (Section IV A) and inclined (Section IV B) substrates. In the latter case we explore in detail the dependence on both the ridge volume and inclination angle. In Section IV C we discuss the physical mechanism of the front and back instabilities using an adaptation of the energy analysis introduced by SPAID and HOMSY[5]. In Section IV D an evolution equation for transverse disturbances of very small wavenumber is derived, and used to explain an unexpected property of the dispersion relation for transverse perturbations on an inclined substrate in the long wavelength limit. Section V summarizes the main results, relates them to the literature and points out possible directions of future research.

II. FILM THICKNESS EQUATION

We start with the evolution equation for the film thickness derived by PISMEN and POMEAU[49] combining the long wave approximation for thin films with a diffuse interface description for the liquid-gas interface:

$$\partial_t h \;=\; -\nabla\cdot\left(Q(h)\left\{\nabla\left[\gamma\Delta h - \partial_h f(h,a)\right] + \vec{e_x}\bar{\alpha}\rho g\right\}\right). \tag{1}$$

Here $h(x,t)$ denotes the film thickness, x denotes the longitudinal (downstream) direction, g is the gravitational acceleration, $Q(h) \equiv h^3/3\eta$ is the mobility factor due to the Poiseuille flow in the film, $\bar{\alpha}$ is the inclination angle between the substrate and the horizontal, and ρ, γ and η are respectively the density, surface tension and (dynamic) viscosity of the liquid. The subscripts t and h denote the corresponding partial derivatives.

Eq. (1) incorporates the Laplace or curvature pressure (first term), driving due to gravity (last term), and the disjoining and hydrostatic pressures contained in the derivative of the free energy $f(h,a)$:

$$\partial_h f(h,a) \;=\; \kappa M(h,a) + \rho g h \;\equiv\; \frac{2\kappa}{a}\,e^{-h/l}\,\left(1 - \frac{1}{a}\,e^{-h/l}\right) + \rho g h. \tag{2}$$

Here $\Pi(h) \equiv -\kappa M(h,a)$ is the disjoining pressure derived from diffuse interface theory[49], a is a small positive parameter describing the wetting properties in the regime of partial wetting, l is the length scale of the diffuse interface, and κ is the strength of the molecular interaction. Except for its behavior for small h the disjoining pressure used here resembles qualitatively other disjoining pressures that combine destabilizing short-range and stabilizing long-range interactions, such as the combination of destabilizing polar and stabilizing apolar interactions that is often used in studies of dewetting[44,47,52,56], or the two antagonistic power law interactions used elsewhere[10,45]. The use of these alternative expressions has no qualitative effect on the results reported below. A similar conclusion for dewetting on a horizontal substrate was established earlier[52].

In the following we use the dimensionless quantities[53] (denoted temporarily by a tilde)

$$\begin{aligned} t &= \frac{\eta\gamma}{\kappa^2 l}\,\tilde{t}, \\ h &= l\,\tilde{h}, \\ x &= \sqrt{\frac{l\gamma}{\kappa}}\,\tilde{x}, \end{aligned} \tag{3}$$

to rewrite Eq. (1) in the form

$$\partial_t h \;=\; -\nabla \cdot \{Q(h)\,[\nabla\,(\Delta h - \partial_h f) + \vec{e}_x \alpha G]\}\,, \tag{4}$$

where

$$\partial_h f = M(h,a) + Gh, \tag{5}$$

$$\alpha = \bar{\alpha}\,\left(\frac{\gamma}{\kappa l}\right)^{1/2}, \tag{6}$$

and

$$G = \frac{l\rho g}{\kappa} \tag{7}$$

measures the relative strength between gravity and molecular interactions. Since the film flows down the upper surface (as opposed to the underside) of the substrate, $G > 0$. Moreover, $Q(h) = h^3/3$ and $M(h,a)$ is given by Eq. (2) with $l = 1$; since $\kappa l/\gamma = O(a^2)$[49] the length scale in the x-direction is l/a. It follows that the effect of inclination is comparable to that of the hydrostatic term when $\alpha \sim 1$, i.e., when $\bar{\alpha} \sim a$. Since a is small this balance occurs only for small inclinations α. This is the case considered in this paper. In the following we use only dimensionless quantities unless otherwise stated.

The parameter a can be incorporated into the mobility factor Q using the transformation $h' = h + \ln\, a$ leading to an equation for h' of the form (4) but with

$$\partial_h f \;=\; 2\,e^{-h}\,\left(1 - e^{-h}\right) \;+\; Gh, \qquad Q(h,a) = (h - \ln a)^3/3. \tag{8}$$

In either form all spatially periodic solutions with spatial period L satisfy

$$\frac{1}{L}\int_0^L h(x,t)\,dx = \bar{h}, \tag{9}$$

where $\bar{h}$ is a constant, hereafter referred to as the *mean* thickness. This quantity therefore measures the volume of liquid in the spatial period L (i.e., the liquid contained in the drop *and* the precursor); since it is a constant it provides a good measure of the notion of volume. In contrast the term drop volume, also used below, refers only to the volume in the drop on top of the precursor film. This quantity is not constant since liquid may flow in and out of a drop at the expense of the precursor. Of course when L contains several drops the volume of one may grow at the expense of another, and as a result the different drops within L may have different volumes.

In the following we solve the problem in the form (8). It is important therefore to remember that the true thickness of the film is $h - \ln a$, i.e., a quantity slightly larger than that computed from Eqs. (4,8). It is appropriate to think of this change in thickness as a change in the thickness of the *precursor*.

The linear stability properties of the flat film solution $h_0(x) = h_0 \equiv \bar{h}$ of Eq. (4) in one dimension are well understood[53,54]. The (one-dimensional) stability properties of spatially periodic solutions have also been extensively investigated[53,54]. On a horizontal substrate these solutions are time-independent, while on an inclined substrate they are stationary only in an appropriately moving reference frame. Such stationary solutions are obtained as solutions of the nonlinear eigenvalue problem

$$0 = Q(h,a)(\partial_{xxx}h - \partial_{hh}f\,\partial_x h) + \alpha G\,Q(h,a) - vh + C_0, \tag{10}$$

for the drift speed v of the solution, measured in units of $(l\kappa)^{3/2}/\eta\sqrt{\gamma}$. Here C_0 is a constant of integration, and is nonzero whenever the substrate inclination is nonzero. For a homogeneous film of thickness h_0 we write

$$C_0 = -(\Gamma_0 - vh_0) = -Q(h_0,a)\,\alpha G + vh_0, \tag{11}$$

where $\Gamma_0 \equiv Q(h_0,a)\,\alpha G$ is the downstream flux of liquid in the laboratory frame. This problem can be solved using continuation techniques, starting from small amplitude steady solutions on a horizontal substrate[53,54]. One finds that, depending on the mean film thickness, different types of solutions may be present. These may be classified into linearly unstable (subcritical) nucleation solutions and linearly stable larger amplitude states. Although for small inclination angles the solution families found correspond to those found on the horizontal substrate[48] there are already some significant differences. First, the solutions are asymmetric and *slide* down the inclined plane. Second, the dependence of the velocity on the solution period varies strongly with the mean film thickness, a behavior that has no counterpart in the horizontal case. In addition, for larger values of α, stationary nonlinear surface waves are present.

The large amplitude stable solutions take the form of (i) small drops whose shape resembles an asymmetric inverted cup whose properties like the drift speed and dynamic contact angles at the front and back depend both on the drop volume and on the inclination angle, or (ii) large flat drops resembling a liquid sheet of constant thickness with a capillary ridge at its front end. Both types of drops sit on a precursor film whose thickness is also given by the model.

In contrast to the small drops the properties of the flat drops do not depend on the volume in the drop[53]. However, with increasing inclination angle the thickness of the film in the plateau region decreases while the precursor film thickness and the drift speed v increase, and the dynamic contact angle at the rear decreases. In contrast the dynamic contact angle at the front shows a nonmonotonic dependence on the speed v: it first increases with v and then decreases and even falls below its static equilibrium value. This effect is more pronounced for larger G. In two dimensions these solutions are independent of the transverse coordinate y and will be referred to as *ridges*.

Fig. 1 shows the transition, for fixed inclination angle and interaction parameters, from a small cup-like drop to a large flat drop as the volume in the drop increases. In two spatial dimensions the cup-like solutions correspond to cross-sections of ridge-like solutions that are independent of the transverse coordinate y (and so are perpendicular to the slope). The flat drops correspond to cross-sections of liquid sheets of finite longitudinal extent. Both solutions are related to appropriate limiting cases already studied in the literature: (i) the front of a long flat drop resembles a single front moving down an inclined plate[5], and (ii) the liquid ridges on a horizontal substrate[26] resemble the small volume drops when the inclination angle approaches zero. The transverse stability properties of these limiting cases are already known; we explore below the corresponding results for drops of finite extent on an inclined substrate, focusing on small but not too small values of G. Existing work in one dimension[53,54] shows that even though G is normally very small qualitatively correct results are obtained already for moderately small values of G. Consequently we limit our study of the two-dimensional problem to such values of G, anticipating that the results will remain qualitatively correct down to physically relevant values of G.

III. LINEAR STABILITY

Having determined the stationary solutions $h_0(x)$ in the comoving frame we now study their linear stability to transverse perturbations. The Ansatz $h(x,y,t) = h_0(x) + \epsilon\, h_1(x)\, \exp(iky + \beta t)$ used in Eqs. (4,8) in the comoving frame leads to a linear eigenvalue problem for the growth rate β of the form

$$\beta h_1(x) = \mathbf{S}(k, h_0(x))\, h_1(x). \tag{12}$$

Here the operator $\mathbf{S}$ is a function of the transverse wavenumber k, and a functional of h_0 and its derivatives, and is given in the Appendix, Eq. (A.9). The eigenvalue problem (12) is solved using a three step procedure. First, h_0 and the speed v are determined, at fixed volume, using numerical continuation techniques[57] starting from analytically known small amplitude solutions, as described elsewhere[53]. The eigenvalue problem is then discretized in space and solved numerically. The necessary equidistant discretization imposes a strong limitation on the parameter range where it can be used. The method gives, for instance, no reliable eigenvalues for large periods ($L > 150$)[53]. To overcome this problem we use, as a third step, the small L results as starting solutions for numerical continuation in L of both h_0 and v, *and* of the solutions to the eigenvalue problem (12). It is convenient to fix the L^2 norm of h_1 during this process. The required extended system consists of 11 first order differential equations (3 for h_0 and 4 each for the real and imaginary parts of h_1). Using this method we determine in parallel the stationary solutions, and the eigenfunctions and eigenvalues of the linear problem (12) for any set of parameter values. Furthermore, points of special interest such as the zeros or the maxima of $\beta(k)$, or the transition between real and complex eigenvalues can be followed through parameter space. The maxima generally occur at $k < 0.1$, implying that the most unstable (dimensional) wavelength is of order $60l/a \gg l$.

IV. RESULTS

A. Horizontal substrate

Instabilities of a liquid ridge on a horizontal substrate ($\alpha = 0$) are characteristic of the dewetting process. In this process an initially thin film may rupture at defects, and the resulting holes grow until they touch one another, creating a polygonal network of straight liquid ridges. It is observed that these ridges decay on a longer time scale forming rows of drops[58,59]. The stability study performed here applies to the individual straight ridges.

Typical cross-sections of such ridges are shown in Fig. 2 (a). These have been computed as steady solutions of Eq. (4) with $\alpha = 0$. For these cases the precursor thickness is given (via a Maxwell construction) by the potential $f(h)$; in contrast on an inclined substrate the precursor thickness depends in addition on the drop velocity and the inclination angle[48,53]. The dispersion relation for transverse perturbations of such a ridge, obtained as described in Section III,

is shown in Fig. 2 (b). It is important to note that there are *two* modes with zero growth rate at $k = 0$: these are the marginally unstable varicose mode and the marginally stable zigzag mode, already discussed by SEKIMOTO et al.[27] using an energy functional. Note that the zero growth rate for the varicose mode at $k = 0$ is a direct consequence of volume conservation: a non-zero growth rate would violate it. The appearance of these modes is sketched in the insets in Fig. 2 (b). Both are related to the neutral modes corresponding to the continuous symmetries of the one-dimensional solution: translation invariance is responsible for the zigzag mode, while invariance with respect to volume change gives rise to the varicose mode. These neutral modes, i.e., the eigenfunctions of the two-dimensional stability problem at $k = 0$, are shown in Fig. 2 (c). Their resemblance to the finite k modes is clear. Note that both dispersion curves vanish quadratically as the transverse wavenumber k approaches zero. As a result each mode is mapped onto itself under $k \to -k$. The eigenfunctions of the two modes are virtually unchanged in the k-range shown in Fig. 2 (b): the modes for $k = 0$ and $k = 0.06$ cannot be distinguished on the scale of Fig. 2 (c). Increasing the drop volume at fixed period by increasing the mean film thickness (cf. Fig. 2 (a)) leads to ridges with cross-sections that resemble flat drop solutions[48]. Such drops are still unstable to the varicose mode, although the maximum growth rate and the corresponding transverse wavenumber both decrease exponentially with increasing volume, measured in Fig. 2 (d) in terms of mean film thickness $\bar{h}$. In practice, therefore, broad ridges are effectively stable on the time scales accessible in experiments.

B. Inclined substrate

The physical situation changes dramatically once $\alpha \neq 0$ as a consequence of the broken symmetry $x \to -x$. As a result the drops become asymmetric and slide down the substrate (on top of the precursor film whose thickness now depends on inclination angle and the drop velocity[53]).

When $\alpha = 0$ the variational structure of Eq. (10) implies that $v = C_0 = 0$. As a result the equation is invariant under both translations in x and changes in volume (or $\bar{h}$). In particular for each set of parameter values there is a two-parameter family of solutions. In contrast, when $\alpha \neq 0$ the stationary solutions are described by Eq. (10) with α, v, and C_0 all nonzero. The resulting equation is still invariant under translation but no longer under volume change. This

is because a change in volume also changes the velocity v. As a result only the translational neutral mode remains, i.e., only one mode with zero growth rate exists at zero wavenumber, in contrast to the two modes for the horizontal substrate. This implies that the two leading eigenmodes of the transverse stability problem, i.e., the equivalents of the varicose and zigzag modes for the inclined case are either no longer independent at $k = 0$ or only one has a zero growth rate at $k = 0$. In fact we find that the first hypothesis is true: the two modes coincide at $k = 0$ forming the translational neutral mode, but are distinct whenever $k \neq 0$ being mapped into one another by the transformation $k \to -k$.

In the following we study the stability of a liquid ridge as a function of both its volume and of the inclination angle.

a. Change of ridge volume The volume of the liquid in the ridge can be changed in two ways. On the one hand the volume in the ridge can be increased [decreased] by increasing [decreasing] the mean film thickness keeping the period fixed. On the other hand one can fix the mean film thickness and increase [decrease] the period. Both procedures lead to identical drops sitting on precursor films of identical thickness but different length, and give identical results for the dispersion relation *unless* the period used is so small that individual ridges in the different periods 'overlap'. For the parameter values used this can be avoided by choosing $L \leq 75$. The results reported below have been obtained in *both* of the above ways and cannot be distinguished on the scale of the figures.

As the volume is increased the ridges with small cup-like cross-section change to large flat drops with a capillary ridge at the front whose profile relaxes towards the upper plateau thickness (see for instance the upper panels of Figs. 3(a-d)). This change in the ridge profile is accompanied by a rather drastic change in the dispersion curves for the two leading eigenvalues (Fig. 4) and the corresponding eigenfunctions (lower panels of Fig. 3). At small volume two dispersion curves, $\beta_1(k)$ and $\beta_2(k)$, are still present, but in contrast to the $\alpha = 0$ case these now cross *linearly* at $k = 0$, implying that $\beta_1(k) = \beta_2(-k)$ and $\beta_1(k) = -\beta_2(k)$. Note in particular that the dominant instability mode (i.e., the mode with maximum growth rate) may now be an asymmetric zigzag mode (dashed line in the lower panel of Fig. 3 (a)), even though for smaller drop volume and very small α the (asymmetric) varicose mode remains dominant (not shown).

With increasing volume the character of the dispersion relation undergoes two consecutive changes (Fig. 4). First, the two dispersion curves approach one another at a finite value of k.

At a certain volume they touch, and for larger volumes there is an interval of wavenumbers $k_{o1} < k < k_{o2}$ in which the growth rate is complex, and real growth rates are present for $k < k_{o1}$ and $k > k_{o2}$ only (Fig. 4 (b)). The complex (oscillatory) mode is initially stable but with increasing volume it acquires an interval of instability which increases until the complex mode is unstable throughout its range of existence. With further increase in volume the real modes at large k also lose stability; at the same time the interval of complex modes shrinks (Fig. 4 (c)), and there is a second critical volume at which the imaginary part of the growth rates vanishes, and the modes become purely real again (Fig. 4 (d)). Note that the maximum growth rate of the oscillatory mode is always smaller than the maximum of the real growth rates so that any instability is dominated by modes that grow monotonically. Thus oscillations may only be expected in laterally confined systems. The net outcome of these changes is to replace the dominant unstable mode at small volumes by a different mode, one that is related to the *stable* mode at small k. In particular, for sufficiently large ridge volumes the former dominates only at small k while the new mode dominates at larger k and has a larger maximum growth rate (Fig. 4 (d)). Neither of these modes resembles the zigzag or the varicose modes present at small volume. Instead, the eigenfunctions at maximum growth rate are localized at the front (the small k mode) or the back (the large k mode) of the ridge. Fig. 4 (d) therefore indicates that for the parameter values considered the instability of the back is always *faster* than the instability of the front. However, because the instability modes at the maxima of the dispersion relation are totally decoupled one may expect that in an experiment on ridges of large volume both instabilities may proceed in parallel, and exhibit different wavelengths and growth rates. These predictions concur with preliminary results from two-dimensional numerical simulations of Eq. (4)[13,54].

To systematize these results we plot in Fig. 5 the growth rates at the two maxima as functions of the ridge volume, using the spatial period as control parameter (at fixed mean thickness). Using the values given in the caption to Fig. 4 as a guide one can "translate" the horizontal axis into mean film thickness $\bar{h}$ at fixed period. As expected both growth rates approach constant values at large periods because the front and back instabilities are then completely decoupled and therefore independent of the length of the drop. The system behavior can be quantified further by tracking the various special wavenumbers (k_{max} for maximum growth rate, k_c for marginal stability and k_o at the transition between real and oscillatory modes) as a function

of the spatial period at fixed mean film thickness (Fig. 6). The most important curves are the heavy dashed (dotted) lines that separate, for real (oscillatory) modes, the unstable wavenumbers (shaded gray) from the stable ones. The thin dashed lines indicate the remaining zero crossings of branches of the dispersion relation (i.e., crossings in the unstable regime), whereas the thin dotted line denotes the limits of existence of the oscillatory modes. The positions of the maxima of the dispersion relation are indicated by the solid lines, with heavy lines indicating the wavenumber of the absolute maximum. It is noteworthy that the critical wavenumber decreases with increasing period in the small volume regime, while it increases (slightly) in the large volume regime towards its value for the completely decoupled back.

b. Change of inclination angle Beside the ridge volume the second control parameter of interest is the inclination angle α of the substrate. At fixed period and a mean film thickness large enough that the one-dimensional steady state for $\alpha = 0$ is a flat drop[48] an increase in α produces sliding drops whose upper plateau is inclined relative to the substrate over all of its length (Fig. 7 (a)). With further increase in α this inclination decreases as the drop develops a capillary ridge at the front and a upper plateau of constant thickness (Fig. 7 (c)). With further increase in α the upper plateau thickness decreases slightly while the precursor film thickness slightly increases (Fig. 7 (c,d)). These changes are reflected in the corresponding changes in the dispersion relation (Fig. 8); these resemble the sequence of changes found when increasing the ridge volume in Section *a* above, but with fastest growing wavenumbers and maximal growth rates that differ by one and two orders of magnitude, respectively.

The stationary solutions and the front and back eigenmodes at maximum growth rate and at $k = 0$ can be found in Fig. 7. At large inclination angle the modes at the two maxima correspond to pure front (small k maximum) and pure back (large k maximum) modes. The maximal growth rates of both modes increase with increasing α as shown in Fig. 9. For smaller α the small k mode is dominant but is eventually overtaken by the large k mode; the latter dominates for $\alpha > 0.15$. Fig. 10 shows the various special wavenumbers identified in Fig. 6 as a function of α for fixed volume. The critical wavenumber k_c increases with α, as do the two fastest growing wavenumbers. This increase is faster for the back mode.

Knowing that on the one hand the two eigenmodes at the maxima in Fig. 4 (d) are localized at the front or the back and that on the other hand at $k = 0$ they both represent the translational neutral mode (a zigzag mode) the question arises how the eigenfunctions change

along the dispersion relations. We visualize this change by plotting in Fig. 11 (a-d) the maximum (or minimum) amplitudes h_{1m} of the eigenfunctions at the front and the back of the ridge for the parameter values corresponding to the dispersion relations in Fig. 8 (a-d). The oscillatory modes are omitted from this plot because they are not important for the analysis. The dashed (solid) lines represent the contributions from the front (back) of the ridge, while the heavy (thin) lines are used to distinguish the two modes using their large k behavior. Thus the heavy (thin) lines refer to what we have called the back (front) modes, or equivalently the large k (small k) modes. The latter terminology is based on Fig. 11 (d), in which the dotted vertical lines mark the k values corresponding to maximum growth rate and the filled circles indicate the corresponding eigenfunction maxima. One sees that in all four panels of Fig. 11 the dashed heavy line approaches zero at large k implying that at large k this mode is not involved in the instability of the front position, i.e., that it is localized at the back. In contrast, the fact that the dashed thin line approaches a finite value while the solid thin line approaches zero implies that the small k mode is localized at the front. If at a certain value of k the values along the thick (or thin) curves are both nonzero and of opposite sign, the corresponding eigenmode represents a zigzag mode, whereas like signs indicate a varicose mode. Thus for $\alpha = 0.025$ the long wave unstable mode (heavy lines near $k = 0$) is a zigzag mode; the anticipated varicose instability occurs for yet smaller values of the inclination (not shown).

One can use Fig. 11 to distinguish four distinct k ranges. (i) The region $k \approx 0$, where the deviation of either mode from the translational neutral mode (a zigzag mode with nearly equal contributions from the front and the back) is linear and can be treated analytically, as in Section IV D. Region (ii) with $0 < k < 0.02$ (see Fig. 11 (a)) where the unstable mode remains of zigzag type but the contribution from the front of the ridge dominates more and more as k increases (heavy lines). The corresponding stable mode is also of zigzag type (thin lines), and for this mode the contribution from the back exceeds that from the front. In region (iii) at $k \approx 0.02$ (Fig. 11 (a)) the relative contribution to either mode from the back falls dramatically. For the unstable mode this contribution changes sign and the mode becomes a varicose one; with increasing k the contribution from the front drops rapidly and at large k this mode is therefore confined to the back of the ridge. In contrast the stable mode remains a zigzag mode but for $k \gtrsim 0.02$ this mode is dominated by the contribution from the front of the ridge. Thus at large k the dominant modes take the form of pure back and front modes (regime (iv)). If we

ignore the narrow k ranges where the eigenmodes are oscillatory the above description, with obvious modifications, also applies to the remaining panels of Fig. 11. The general tendency is towards a narrowing of the transition regions (i) and (iii) with increasing ridge volume, with the provison that at the same time the wavenumbers corresponding to maximum growth rates move from range (i) to (iv). Thus for sufficiently large ridge volumes (and inclination angles) the dominant *unstable* modes are localized at the front and back of the ridge.

C. Physical mechanism

The physical mechanism responsible for contact line instabilities can be studied using the widely used method of *energy analysis*[5,21,22,60]. The growth rate β of an unstable mode is interpreted as an energy production rate and contributions to it from the individual terms of the linearized problem can be connected to underlying physical mechanisms[5]. For this type of analysis we multiply Eq. (12) by h_1 and integrate the result over one spatial period. The right side then consists of a sum of the individual contributions, β_n, defined by

$$\beta_n = -\frac{\langle h_1, \mathbf{S}_n h_1 \rangle}{\langle h_1, h_1 \rangle}, \tag{13}$$

where

$$\langle v, w \rangle = \int_0^L vw \, dx. \tag{14}$$

The operators $\mathbf{S}_n$ that add up to give the linear operator $\mathbf{S}$ are given, together with their physical interpretation, in Table I and depend nonlinearly on the base flow solution $h_0(x)$.

The assessment of the influence of the individual terms, used in the literature, is based on the signs of the respective β_n: positive β_n are destabilizing, while terms corresponding to negative β_n are stabilizing[5,21,22]. Although this interpretation provides useful information about the overall influence of the terms it does not reveal either the mechanism of the instability or the terms responsible for the selected wavenumber because it does not take into account that all the contributions β_n in fact balance at $k = 0$: $\sum \beta_n(k = 0) = 0$. This requirement is a consequence of the fact that at $k = 0$ the unstable mode becomes the translational neutral mode of the one-dimensional geometry. It is the destabilization of this mode, and therefore the *deviation* of the β_n from their values at $k = 0$ that determines the transverse instability[60]. Hence the most important instability mechanisms are those for which the associated β_n deviate most

from their value at $k = 0$. These deviations are plotted in Figs. 12 (a) and (b) for the back and front mode, respectively (parameter values as in Fig. 4 (d)).

Fig. 12 reveals rather drastic changes in the individual contributions near $k = 0$ (both modes) and $k = 0.05$ (back mode). These correspond to the qualitative changes in the eigenmodes around these k values noted already in Fig. 11. Thus as formulated here the energy analysis is capable of revealing more detailed information than its traditional version[5,21,22]. A second difference between the present problem and those studied in the literature arises from the fact that contributions to β_n, for either mode, can arise from the front, β_n^f, and the back, β_n^b, if the eigenfunction has two peaks. So a situation may arise where $\beta \equiv \beta^f + \beta^b$ is dominated by either the front or the back, but the individual contributions to these, β_n^f or β_n^b, may bear no relation to the location of the dominant instability. Here we have introduced

$$\beta_n^b = \langle h_1, \mathbf{S}_n h_1 \rangle_b / \langle h_1, h_1 \rangle, \qquad \beta_n^f = \langle h_1, \mathbf{S}_n h_1 \rangle_f / \langle h_1, h_1 \rangle, \tag{15}$$

where

$$\langle v, u \rangle_b = \int_0^\xi vu \, dx, \qquad \langle v, u \rangle_f = \int_\xi^L vu \, dx, \tag{16}$$

respectively, with ξ chosen to lie between the locations of the back and the front. For drops of sufficiently large volume the exact value of the cut $x = \xi$ becomes immaterial and the quantities β_n^f, β_n^b become independent of ξ. Figs. 13 (a) and (b) show β, β^f and β^b for the front and back mode, respectively. These show clearly that the front mode is exclusively caused by contributions from the front part of the profile even in the range at very small k for which the eigenfunction has significant amplitude at both the front and the back. In this case all but one of the signs of the β_n^f agree with the signs of the corresponding β_n. Likewise, the back mode is mainly caused by contributions from the back part of the profile (Fig. 13 (b)). However, during the qualitative change in the eigenfunction near $k = 0.05$ the instability is briefly dominated by contributions from the front. For the back mode the split of the β_n into the β_n^f and β_n^b has a profound effect on the signs of the individual contributions as can be seen when comparing Fig. 14 with Fig. 12 (b).

The overall influence of the individual terms is summarized in Table II. Comparison of the contributions from the front part of the front mode (column 3) with the contributions from the back part of the back mode (column 4) indicates that in both cases the main stabilizing influence comes from term 2, i.e., the flow in the x-direction due to x-curvature, and the main

destabilizing influence from term 8, i.e., the flow in the x-direction due to variations of the disjoining pressure. The hydrostatic pressure terms are stabilizing for both instabilities, whereas the flow in the y-direction due to variations of the disjoining pressure (term 10) is destabilizing. The two instabilities differ only in terms 4 and 5, that are both destabilizing for the front and stabilizing for the back. However, of these term 5 is relatively unimportant, while term 4 arises from the flow in the x-direction due to the body force, one of the two most destabilizing terms in the model of SPAID and HOMSY in either interpretation of the energy analysis[60].

D. Analytical approach

As already mentioned the dispersion curves undergo a remarkably transition near $k = 0$ as soon as α becomes nonzero. To understand the origin of this change we introduce two slow timescales, $\tau = \epsilon t$ and $T = \epsilon^2 t$, and a long transverse scale $Y = \epsilon y$, where $\epsilon \ll 1$, so that $\partial_t = \epsilon\partial_\tau + \epsilon^2\partial_T$ and $\partial_y = \epsilon\partial_Y$. Next we suppose that the film thickness can be written in the form

$$h = h_0(x + \theta(Y, \tau, T)) \, + \, \epsilon \, h_1(x, Y, \tau, T) \, + \, \epsilon^2 \, h_2(x, Y, \tau, T) \, + \, O(\epsilon^3), \tag{17}$$

where

$$\theta \, = \, \theta_0 + \epsilon\theta_1 + \epsilon^2\theta_2 \, + \, O(\epsilon^3) \tag{18}$$

is a slowly varying spatial phase, and h_1 and h_2 represent perturbations of the drop. With this Ansatz the left hand side of Eq. (4) becomes

$$h_t \, = \, h_{0x}(\epsilon\theta_\tau + \epsilon^2\theta_T) \, + \, \epsilon^2 h_{1\tau} \, + \, \epsilon^3 h_{1T} \, + \, \epsilon^3 h_{2\tau} \, + \, O(\epsilon^4). \tag{19}$$

The nonlinear differential operator $N[h]$ on the right hand side of Eq. (4) (in the comoving frame) can also be written as a series in ϵ. Writing $N = N_0 + N_2 + N_4$, where N_0 denotes the part that does not contain derivatives with respect to Y, N_2 denotes terms with two such derivatives, and N_4 denotes terms with four derivatives, we find that

$$N[h] \, \equiv \, N[h_0{+}\epsilon h_1{+}\epsilon^2 h_2] \, = \, N_0[h_0]{+}\epsilon N_{0h}[h_1]{+}\frac{1}{2}\epsilon^2 N_{0hh}[h_1]{+}\epsilon^2 N_{0h}[h_2]{+}\epsilon^2 N_2[h_0] + O(\epsilon^3), \tag{20}$$

where N_{0h} is a linear operator depending on h_0 and acting here on h_1 or h_2 and N_{0hh} is a nonlinear operator depending on h_0 and involving terms quadratic in h_1. From the Ansatz for

h_0 (Eq. (17)) $N_2[h_0]$ can be written in the form $\theta_{YY} N_{2a}[h_0(x)] + \theta_Y^2 N_{2b}[h_0(x)]$. All of the above operators are summarized in the Appendix.

At leading order one now obtains the equation $0 = N_0[h_0]$ for the one-dimensional stationary solutions. Order ϵ yields

$$h_{0x}\theta_{0\tau} \;=\; N_{0h}[h_1]. \tag{21}$$

Note that the $O(\epsilon)$ equation does not yield the translational neutral mode h_{0x} because this mode is already included in the Ansatz for $h_0 = h_0(x+\theta)$. The linear inhomogeneous equation (21) for h_1 has a solution if and only if

$$0 \;=\; \int g^+ N_{0h}[h_1]\, dx \;=\; \theta_{0\tau} \int g^+ h_{0x}\, dx, \tag{22}$$

where g^+ is the eigenfunction of the adjoint operator N_{0h}^+ (see Appendix) corresponding to the eigenfunction h_{0x} of N_{0h}. Inspection of N_{0h}^+ shows that g^+ is a constant implying that the solvability condition is trivially fulfilled (since $\int h_{0x} dx = 0$). Thus N_{0h} has a unique inverse, and

$$h_1 = \theta_{0\tau} N_{0h}^{-1}[h_{0x}] \tag{23}$$

can be calculated from h_{0x}. To order ϵ^2 one finds

$$h_{1\tau} + h_{0x}\theta_{0T} + h_{0x}\theta_{1\tau} \;=\; \frac{1}{2} N_{0hh}[h_1] + N_{0h}[h_2] + N_2[h_0]. \tag{24}$$

This is an inhomogeneous equation for h_2. The solvability condition, obtained by multiplying by g^+ and integrating over $0 < x < L$ yields the desired envelope equation. Using Eq. (23) and the fact that $\int h_{0x}\, dx = 0$ this equation takes the form

$$a_1 \theta_{0\tau\tau} \;=\; a_2 \theta_{0\tau}^2 + a_3 \theta_{0Y}^2 + a_4 \theta_{0YY}, \tag{25}$$

where

$$\begin{aligned} a_1 \;&=\; \int N_{0h}^{-1}[h_{0x}]\, dx && (26)\\ a_2 \;&=\; \frac{1}{2} \int N_{0hh}[N_{0h}^{-1}[h_{0x}]]\, dx \\ a_3 \;&=\; \int N_{2b}[h_0]\, dx \\ a_4 \;&=\; \int N_{2a}[h_0]\, dx. && (27) \end{aligned}$$

The linearization of Eq. (25),

$$a_1\theta_{0\tau\tau} \;=\; a_4\theta_{0YY}, \tag{28}$$

now gives the desired dispersion relation valid near $k = 0$, viz. $a_1\beta^2 + a_4k^2 = 0$, implying the presence of two branches of the dispersion relation $\beta(k)$ crossing the axis $k = 0$ linearly at $\beta = 0$. The slope $\beta'(k)$ at $k = 0$ is given by $\pm\sqrt{-a_4/a_1}$, a quantity that can be computed for a given stationary profile h_0 from the formulae (26,27). Fig. 15 demonstrates excellent agreement between the above prediction and the full dispersion relation computed directly from Eq. (12). As the inclination α of the substrate decreases towards zero so does the coeffient a_4. As this occurs the scaling assumed above breaks down and fourth order derivatives enter the leading order balance in the dispersion relation, resulting in a dramatic change in the dispersion relation.

V. CONCLUSION

In this paper we studied the transverse instability of liquid ridges on horizontal and inclined substrates using a film evolution equation based on a long wave approximation, incorporating a disjoining pressure to account for the effective interaction of the film with the substrate. The disjoining pressure used was recently derived by PISMEN and POMEAU using diffuse interface theory[49]. The form of the disjoining pressure that results remains nonsingular even for zero film thickness, and is therefore convenient for analytical study. However, we expect qualitatively similar results for other forms of the disjoining pressure involving a destabilizing short range and a stabilizing long range interaction as occurs for dewetting[52].

We have studied three different types of transverse instabilities for liquid ridges:

(i) The varicose instability on a horizontal substrate involving symmetrically both edges of the ridge. In this situation the competing zigzag mode is stable.

(ii) Coupled instabilities of the front and back of the ridge on an inclined substrate. These are mostly of an asymmetric zigzag type but an asymmetric varicose instability also occurs for very small inclination angles. These instabilities, in which the behavior of the front and back is coupled, are found for small volumes of the ridge or small inclination angles of the substrate.

(iii) Decoupled instabilities of the front and back having different growth rates and fastest growing wavenumbers. These occur for large volumes or large inclination angles.

These instabilities and the transitions between them were studied as a function of the system parameters by means of a linear stability analysis of stationary one-dimensional solutions. Both the stationary solutions and their stability properties can be followed simultaneously in parameter space using numerical continuation techniques[57]. In the transition region between the instabilities (i) - (iii) oscillatory instabilities are present in a certain wavenumber range. However, in the cases studied the oscillatory modes were never dominant, and may therefore be seen only when the corresponding wavenumber is selected by the experimental apparatus.

The mechanisms responsible for the pure back and front instabilities were elucidated using an adaptation of the energy analysis originally proposed by SPAID and HOMSY[5]. The main destabilizing effect in both cases is given by the flow in the longitudinal direction due to the variation of the disjoining pressure caused by the perturbation, while the main difference between the two instabilities arises from the body force that is destabilizing at the front and stabilizing at the back, as in Ref. 5.

The linear stability problem of a finite ridge is characterized by a double zero eigenvalue at $k = 0$. On a horizontal substrate these eigenvalues are a consequence of the two neutral modes of the system, arising from translation invariance in the logitudinal direction and invariance with respect to changes in the mean film thickness. We have seen that for nonzero transverse wavenumber k these eigenvalues become nonzero and depend on k quadratically. This property is a consequence of the invariance of the system under reflection. We have identified the resulting unstable mode with the varicose mode and the stable mode with the zigzag mode. Thus both the algebraic and the geometric multiplicity of the zero eigenvalue is two. In contrast, once the substrate is inclined the algebraic multiplicity of the zero eigenvalue remains two but the geometric multiplicity drops to one: the two dispersion curves cross linearly at the origin where the unstable and stable modes degenerate into one another. We have derived an amplitude equation for the time evolution of transverse perturbations of a sliding ridge on an inclined plane to demonstrate this fact analytically, and showed that this equation reproduces quantitatively the wavenumber dependence of the dispersion relation near the origin. The crossing is a direct result of the breaking of the reflection symmetry that occurs when the substrate is inclined from the horizontal.

The transverse instability of a liquid ridge on a horizontal substrate was studied earlier by DAVIS[26], SEKIMOTO, OGUMA and KAWASAKI[27], and ROY and SCHWARTZ[28], focusing on ridges of heights smaller than the capillary length in order to neglect gravitational effects. Such ridges are always unstable, with the product of ridge width and the critical transverse wavenumber decreasing monotonically from about 2.4 for zero contact angle to zero at a contact angle of 180°[28]. Estimates of this product for the ridges shown in Fig. 2 give values of about 3.4 ($\bar{h} = 0.8$), 2.1 ($\bar{h} = 1.0$) and 0.33 ($\bar{h} = 1.6$). The first two of these values are in good agreement with the literature value for small contact angles (viz., 2.4), especially since the small drops involved are strongly influenced by the destabilizing disjoining pressure used here. The third value is for a ridge that is already flattened by gravity and reveals the stabilizing influence of hydrostatic pressure.

We remark that the variational formulation employed in Ref. 27 yields results that differ from ours. To determine the stability of the ridge the authors examine the variation of the generalized forces with respect to contact line replacements for the varicose and zigzag modes. Negative eigenvalues of the resulting matrix imply instability, and their dependence on the transverse wavenumber k yields information about the most dangerous mode, i.e., the mode with maximal energy gain. The authors of Ref. 27 argue that the eigenvalue of the matrix corresponding to the unstable varicose mode approaches quadratically a nonzero value as k vanishes, implying that the most dangerous mode is of the order of the system size. However, due to volume conservation the authors exclude the point $k = 0$ from this curve. The difference between this result and ours (a quartic relation going to zero as k^2, see Fig. 2 (b)) appears to be due to the intrinsic difference between their static approach involving the study of an energy functional and the dynamical approach we pursue here that takes into account the viscous character of the fluid that suppresses the motion of the liquid on very large scales. Refs. 26, 28 do not compute equivalent dispersion (or eigenvalue) relations.

Our results for small inclination angles or small ridge volumes can be compared with earlier work[25]. The product of the ridge width and the most dangerous wavenumber is in both cases approximately one (cf. Figs. 3 (a) and 4 (a) or Figs. 7 (a) and 8 (a)). However, the transition to large flat ridges with increasing inclination or ridge volume decreases this product by an order of magnitude, although inspection of Figs. 3 (d) and 4 (d) or Figs. 7 (d) and 8 (d) reveals that in this case the product of the width of the *capillary ridge* at the front and the most dangerous

wavenumber of the front mode still remains of order one, as observed in other studies of front instabilities[5,7,18]. However, in contrast to Ref. 25, we find that even for quite small inclination angles or ridge volumes the dominant mode is an asymmetric zigzag mode, with an asymmetric varicose mode found only for very small inclination angles. The transition towards stability found in Ref. 7 for an individual front with decreasing inclination angle is reflected here by the transition between decoupled front and back instability and coupled instabilities. The decoupled front instability has a counterpart in studies of an individual front, the coupled instabilities do not.

Note that for the instability of the back the product of the back width and of the most dangerous wavenumber is also about one. To our knowledge there are currently no experimental investigations of back instabilities for wide ridges or receding fronts on inclined planes. However, a transverse back instability occurs in dewetting, where a liquid recedes on a solid substrate[58,61]. There the mechanism proposed here may play a role although the instability is believed in the literature to be a combination of a Rayleigh instability of the liquid rim formed at the receding back and an instability due to the slip at the substrate[61]. Related work on the stability of a receding dewetting front under evaporation, including the effects of a disjoining pressure, can be found in Ref. 62. Here, too, the presence of the instability is believed to be associated with the forming rim. However, the rim is tiny and it may be that the instability is in fact due to the disjoining pressure, as in the problem studied here. Further studies involving an energy analysis of this type of instability are necessary to decide this issue.

We conclude with a few remarks about the possible nonlinear states that may result from the instabilities discussed here. When $\alpha = 0$ and the drop volume is small the unstable varicose mode grows monotonically and may saturate at a finite amplitude, forming a fingered state. If such a state remains unstable the continued growth of the instability will break the ridge into drops which may merge on a longer timescale forming finally a single drop. On an inclined substrate the growth of the fingers, be they varicose or zigzag in structure, affects the speed with which the ridge slides. This effect remains small when the transverse perturbation is small, but the nonvariational structure of the system for $\alpha > 0$ now permits the occurrence of parity-breaking bifurcations producing varicose, zigzag or mixed modes that drift in the transverse direction; these in turn can lead to complex dynamical behavior, as discussed elsewhere[63,64]. Fig. 4 (d) suggests another source of complex dynamics as well. The figure shows that the

maximum growth rate of the varicose mode occurs near $k = k_0 \equiv 0.035$ while that of the zigzag mode occurs near $k = 2k_0$. Since the ridge has the symmetry O(2) in the transverse direction, generated by translations $y \to y + c$ and reflection $y \to -y$, the resulting mode interaction corresponds to the $1 : 2$ spatial resonance in the presence of O(2) symmetry, at least if periodic boundary conditions with spatial period $2\pi/k_0$ are imposed in this direction. Recent work indicates the presence of a remarkable wealth of dynamical behavior generated by this mode interaction[65,66]. For other parameter values lateral boundaries may select a primary oscillatory instability, and this may evolve into a pattern of standing oscillations; with periodic lateral boundary conditions with an appropriate period waves that travel either in the $+y$ or the $-y$ directions become possible, and these resemble the laterally drifting states produced in the secondary parity-breaking bifurcations. Distinct dynamical behavior is present near the codimension-two Takens-Bogdanov bifurcations with O(2) symmetry whose presence is also suggested by Fig. 4; at these bifurcations the oscillation frequency vanishes, and the bifurcation therefore represents the transition between an oscillatory and a steady state primary bifurcation. Such bifurcations are, however, accessible only through selecting an appropriate slope α and spatial period $2\pi/k_{TB}$. Simulations of an unstable ridge in two dimensions are likely, therefore, to generate a plethora of new types of behavior that may be relevant to thin film instabilities.

APPENDIX

The nonlinear operators N_0, N_2, and N_4 are given by

$$N_0[h] = -\{Q\,[(h_{xx} - f_h)_x + \alpha G]\}_x + v h_x \tag{A.1}$$

$$N_2[h] = -\{Q\,h_{YYx}\}_x - \{Q\,(h_{xx} - f_h)_Y\}_Y \tag{A.2}$$

$$N_4[h] = -\{Q\,h_{YYY}\}_Y\,, \tag{A.3}$$

where $Q = h^3/3$ and f_h is given by Eq. (8). The time-independent equation $N_0[h] = 0$ gives, after integration and transformation into comoving coordinates, the equation for the stationary states (10). Taking into account that $h_0 = h_0(x + \theta(Y, \tau, T))$, $N_2[h_0]$ can be written as $N_2[h_0] = N_{2a}[h_0]\,\theta_{YY} + N_{2b}[h_0]\,\theta_Y^2$ with

$$N_{2a}[h_0] = -\{Q\,h_{0xx}\}_x - Q\,(h_{0xx} - f_h)_x \tag{A.4}$$

$$N_{2b}[h_0] = -\{Q\,h_{0xxx}\}_x - \{Q\,(h_{0xx} - f_h)_x\}_x\,. \tag{A.5}$$

Using the Ansatz $h = h_0(x) + \epsilon u(x, Y)$ where $\epsilon \ll 1$ and u is a perturbation, the linearized operators N_{0h}, N_{2h} and N_{4h} are

$$\begin{aligned} N_{0h}[u] &= -\left\{Q_h u\left[(h_{0xx} - f_h)_x + \alpha G\right]\right\}_x + v u_x \\ &\quad -\left\{Q\left(u_{xx} - f_{hh} u\right)_x\right\}_x \qquad \text{(A.6)} \\ N_{2h}[u] &= -\left\{Q\, u_{xYY}\right\}_x - Q\left(u_{xxYY} - f_{hh} u_{YY}\right) \qquad \text{(A.7)} \\ N_{4h}[u] &= -Q\, u_{YYYY}, \qquad \text{(A.8)} \end{aligned}$$

where $Q = (h_0(x) - \ln a)^3/3$ and all derivatives of f are functions of $h_0(x)$. The linear operator **S** used in the numerical calculations (Eq. (12)) is given by

$$\mathbf{S} = N_{0h} + N_{2h} + N_{4h}, \qquad \text{(A.9)}$$

with each derivative with respect to Y in N_{2h} and N_{4h} replaced by the factor ik. The adjoint operator, N_{0h}^+, of the linear operator N_{0h} defined by $\langle w, N_{0h}[u]\rangle = \langle N_{0h}^+[w], u\rangle$ is given by

$$N_{0h}^+[w] = Q_h\left(\left[h_{0xx} - f_h\right]_x + \alpha G\right) w_x - v w_x - (Q w_x)_{xxx} + f_{hh}\,(Q w_x)_x. \qquad \text{(A.10)}$$

For the eigenvalue zero the eigenfunction is given by $w_x = 0$, i.e., the adjoint eigenfunction for the neutral mode of N_{0h} is a constant.

Finally, the leading nonlinear operator N_{hh} is given by

$$\begin{aligned} N_{hh}[u] &= -\left\{Q_h u\left(u_{xx} - f_{hh} u\right)_x\right\}_x \\ &\quad -\left\{Q_{hh} u^2\left[(h_{0xx} - f_h)_x + \alpha G\right]\right\}_x \\ &\quad +\left\{Q\left(f_{hhh} u^2\right)_x\right\}_x. \qquad \text{(A.11)} \end{aligned}$$

[1] H. E. Huppert, "Flow and instability of a viscous current down a slope," Nature **300**, 427–429 (1982).

[2] L. W. Schwartz, "Viscous flows down an inclined plane: Instability and finger formation," Phys. Fluids A **1**, 443–445 (1989).

[3] S. M. Troian, E. Herbolzheimer, S. A. Safran, and J. F. Joanny, "Fingering instabilities of driven spreading films," Europhys. Lett. **10**, 25–30 (1989).

[4] J. R. de Bruyn, "Growth of fingers at a driven three–phase contact line," Phys. Rev. A **46**, R4500–R4503 (1992).

[5] N. A. Spaid and G. M. Homsy, "Stability of newtonian and viscoelastic dynamic contact lines," Phys. Fluids **8**, 460–478 (1996).

[6] M. A. Spaid and G. M. Homsy, "Stability of viscoelastic dynamic contact lines: an experimental study," Phys. Fluids **9**, 823–832 (1997).

[7] A. L. Bertozzi and M. P. Brenner, "Linear stability and transient growth in driven contact line," Phys. Fluids **9**, 530–539 (1997).

[8] I. Veretennikov, A. Indeikina, and H. C. Chang, "Front dynamics and fingering of a driven contact line," J. Fluid Mech. **373**, 81–110 (1998).

[9] Y. Ye and H.-C. Chang, "A spectral theory for fingering on a prewetted plane," Phys. Fluids **11**, 2494–2515 (1999).

[10] M. Eres, L. Schwartz, and R. Roy, "Fingering phenomena for driven coating films," Phys. Fluids **12**, 1278–1295 (2000).

[11] S. Kalliadasis, "Nonlinear instability of a contact line driven by gravity," J. Fluid Mech. **413**, 355–378 (2000).

[12] J. A. Diez and L. Kondic, "Contact line instabilities of thin liquid films," Phys. Rev. Lett. **86**, 632–635 (2001).

[13] M. Bestehorn and K. Neuffer, "Surface patterns of laterally extended thin liquid films in three dimensions," Phys. Rev. Lett. **87**, 046101,1–4 (2001).

[14] A. M. Cazabat, F. Heslot, S. M. Troian, and P. Carles, "Fingering instability of thin spreading films driven by temperature gradients," Nature **346**, 824–826 (1990).

[15] D. E. Kataoka and S. M. Troian, "A theoretical study of instabilities at the advancing front of thermally

driven coating films," J. Colloid Interface Sci. **192**, 350–362 (1997).

[16] D. E. Kataoka and S. M. Troian, "Stabilizing the advancing front of thermally driven climbing films," J. Colloid Interface Sci. **203**, 335–344 (1998).

[17] A. L. Bertozzi, A. Münch, X. Fanton, and A. M. Cazabat, "Contact line stability and "undercompressive shocks" in driven thin film flow," Phys. Rev. Lett. **81**, 5169–5173 (1998).

[18] A. A. Golovin, B. Y. Rubinstein, and L. M. Pismen, "Effect of van der Waals interactions on the fingering instability of thermally driven thin wetting films," Langmuir **17**, 3930–3936 (2001).

[19] S. Troian, X. Wu, and S. Safran, "Fingering instability in thin wetting films," Phys. Rev. Lett. **62**, 1496—1499 (1989).

[20] S. Troian, E. Herbolzheimer, and S. Safran, "Model for the fingering instability of spreading surfactant drops," Phys. Rev. Lett. **65**, 333–336 (1990).

[21] O. Matar and S. M. Troian, "Linear stability analysis of an insoluble surfactant monolayer spreading on a thin liquid film." Phys. Fluids **9**, 3645–3657 (1997).

[22] O. K. Matar and S. M. Troian, "Growth of non-modal transient structures during the spreading of surfactant coated films," Phys. Fluids **10**, 1234–1236 (1998).

[23] M. Cachile and A. M. Cazabat, "Spontaneous spreading of surfactant solutions on hydrophilic surfaces: C_nE_m in ethylene and diethylene glycol," Langmuir **15**, 1515–1521 (1999).

[24] L. M. Hocking, "Spreading and instability of a viscous-fluid sheet," J. Fluid Mech. **211**, 373–392 (1990).

[25] L. M. Hocking and M. J. Miksis, "Stability of a ridge of fluid," J. Fluid Mech. **247**, 157–177 (1993).

[26] S. H. Davis, "Moving contact lines and rivulet instabilities. Part 1. The static rivulet," J. Fluid Mech. **98**, 225–242 (1980).

[27] K. Sekimoto, R. Oguma, and K. Kawasaki, "Morphological stability analysis of partial wetting," Ann. Phys. **176**, 359–392 (1987).

[28] R. V. Roy and L. W. Schwartz, "On the stability of liquid ridges," J. Fluid Mech. **391**, 293–318 (1999).

[29] Lord Rayleigh, "On the stability of jets," in "Scientific Papers I," pages 361–371 (Cambridge, England, 1899).

[30] S. Chandrasekhar, *Hydrodynamic and Hydromagnetic Stability*, Clarendon Press, Oxford (1961).

[31] C. Huh and L. E. Scriven, "Hydrodynamic model of steady movement of a solid / liquid / fluid contact line," J. Coll. Interface Sci. **35**, 85 (1971).

[32] L. Hocking, "A moving fluid interface. II. The removal of the force singularity by a slip flow," J. Fluid Mech. **79**, 209–229 (1977).

[33] H. Greenspan, "On the motion of a small viscous droplet that wets a surface (relevant to cell movement)," J. Fluid Mech. **84**, 125–143 (1978).

[34] E. B. Dussan, "Spreading of liquids on solid-surfaces - static and dynamic contact lines," Ann. Rev. Fluid Mech. **11**, 371–400 (1979).

[35] P. de Gennes, "Wetting: Statistics and dynamics," Rev. Mod. Phys. **57**, 827–863 (1985).

[36] D. Moyle, M.-S. Chen, and G. Homsy, "Nonlinear rivulet dynamics during unstable wetting flows," Int. J. Multiphase Flow **25**, 1243–1262 (1999).

[37] Y. D. Shikhmurzaev, "Moving contact lines in liquid/liquid/solid systems," J. Fluid Mech. **334**, 211–249 (1997).

[38] B. V. Derjaguin, N. V. Churaev, and V. M. Muller, *Surface Forces*, Consultants Bureau, New York (1987).

[39] G. F. Teletzke, H. T. Davis, and L. E. Scriven, "Wetting hydrodynamics," Rev. Phys. Appl. **23**, 989–1007 (1988).

[40] R. J. Hunter, *Foundation of Colloid Science*, volume 1, Clarendon Press, Oxford (1992).

[41] J. N. Israelachvili, *Intermolecular and Surface Forces*, Academic Press, London (1992).

[42] V. M. Starov, "Equilibrium and hysteresis contact angles," Adv. Colloid Interface Sci. **39**, 147–173 (1992).

[43] V. S. Mitlin, "Dewetting of solid surface: Analogy with spinodal decomposition," J. Colloid Interface Sci. **156**, 491–497 (1993).

[44] A. Sharma and R. Khanna, "Pattern formation in unstable thin liquid films," Phys. Rev. Lett. **81**, 3463–3466 (1998).

[45] A. Oron, "Three-dimensional nonlinear dynamics of thin liquid films," Phys. Rev. Lett. **85**, 2108–2111 (2000).

[46] A. L. Bertozzi, G. Grün, and T. P. Witelski, "Dewetting films: Bifurcations and concentrations," Nonlinearity **14**, 1569–1592 (2001).

[47] U. Thiele, M. G. Velarde, and K. Neuffer, "Dewetting: Film rupture by nucleation in the spinodal regime," Phys. Rev. Lett. **87**, 016104, 1–4 (2001).

[48] U. Thiele, M. G. Velarde, K. Neuffer, and Y. Pomeau, "Film rupture in the diffuse interface model

coupled to hydrodynamics," Phys. Rev. E **64**, 031602, 1–14 (2001).

[49] L. M. Pismen and Y. Pomeau, "Disjoining potential and spreading of thin liquid layers in the diffuse interface model coupled to hydrodynamics," Phys. Rev. E **62**, 2480–2492 (2000).

[50] A. Oron, S. H. Davis, and S. G. Bankoff, "Long-scale evolution of thin liquid films," Rev. Mod. Phys. **69**, 931–980 (1997).

[51] D. M. Anderson, G. B. McFadden, and A. A. Wheeler, "Diffuse-interface methods in fluid mechanics," Annu. Rev. Fluid Mech. **30**, 139–165 (1998).

[52] U. Thiele, K. Neuffer, Y. Pomeau, and M. G. Velarde, "On the importance of nucleation solutions for the rupture of thin liquid films," Colloid Surf. A **206**, 135–155 (2002).

[53] U. Thiele, M. G. Velarde, K. Neuffer, M. Bestehorn, and Y. Pomeau, "Sliding drops in the diffuse interface model coupled to hydrodynamics," Phys. Rev. E **64**, 061601, 1–12 (2001).

[54] U. Thiele, K. Neuffer, M. Bestehorn, Y. Pomeau, and M. G. Velarde, "Sliding drops on an inclined plane," Colloid Surf. A **206**, 87–104 (2002).

[55] T. Podgorski, J.-M. Flesselles, and L. Limat, "Corners, cusps, and pearls in running drops," Phys. Rev. Lett. **87**, 036102, 1–4 (2001).

[56] A. Sharma, "Relationship of thin film stability and morphology to macroscopic parameters of wetting in the apolar and polar systems," Langmuir **9**, 861–869 (1993).

[57] E. J. Doedel, A. R. Champneys, T. Fairgrieve, Y. Kuznetsov, B. Sandstede, and X. Wang, *AUTO97: Continuation and bifurcation software for ordinary differential equations*, Concordia University, Montreal (1997).

[58] A. Sharma and G. Reiter, "Instability of thin polymer films on coated substrates: Rupture, dewetting and drop formation," J. Colloid Interface Sci. **178**, 383–399 (1996).

[59] M. Mertig, U. Thiele, J. Bradt, D. Klemm, and W. Pompe, "Dewetting of thin collagenous precursor films," Appl. Phys. A **66**, S565–S568 (1998).

[60] J. Skotheim, U. Thiele, and B. Scheid, "On the instability of a falling film due to localized heating," J. Fluid Mech. (2002), accepted.

[61] G. Reiter and A. Sharma, "Auto-optimization of dewetting rates by rim instabilities in slipping polymer films," Phys. Rev. Lett. **8716**, 166103, 1–4 (2001).

[62] A. V. Lyushnin, A. A. Golovin, and L. M. Pismen, "Fingering instability of thin evaporating liquid films," Phys. Rev. E **65**, 021602,1–7 (2002).

[63] P. Hirschberg and E. Knobloch, "Zigzag and varicose instabilities of a localized stripe pattern," Chaos **3**, 713–721 (1993).

[64] P. Hirschberg and E. Knobloch, "A robust heteroclinic cycle in an o(2)xz(2) steady-state mode interaction," Nonlinearity **11**, 89–104 (1998).

[65] D. Armbruster, J. Guckenheimer, and P. Holmes, "Heteroclinic cycles and modulated travelling waves in systems with O(2) symmetry," Physica D **29**, 257–282 (1988).

[66] J. Porter and E. Knobloch, "New type of complex dynamics in the 1:2 spatial resonance," Physica D **159**, 125–154 (2001).

Term	Expression	Physical Mechanism
1	vh_{1x}	Convective flow in x-direction due to reference velocity v
2	$\frac{1}{3}(h_0^3 h_{1xxx})_x$	Capillary flow in x-direction induced by perturbation curvature in x-direction
3	$-\frac{1}{3}(k^2 h_0^3 h_{1x})_x$	Capillary flow in x-direction induced by perturbation curvature in y-direction
4	$\alpha G(h_0^2 h_1)_x$	Flow in x-direction due to gravity
5	$(h_0^2 h_{0xxx} h_1)_x$	Capillary flow in x-direction due to perturbation thickness variations
6	$-\frac{1}{3}k^2 h_0^3 h_{1xx}$	Capillary flow in y-direction induced by perturbation curvature in x-direction
7	$\frac{1}{3}k^4 h_0^3 h_1$	Capillary flow in y-direction induced by perturbation curvature in y-direction
8	$(h_0^3 \tilde{f}_{hh} h_1)_{xx}$	Flow in x-direction due to variation of disjoining pressure
9	$G(h_0^3 h_1)_{xx}$	Flow in x-direction due to variation of hydrostatic pressure
10	$-h_0^3 \tilde{f}_{hh} k^2 h_1$	Flow in y-direction due to variation of disjoining pressure
11	$(h_0^3 \tilde{f}_{hh} h_1)_{xx}$	Flow in y-direction due to variation of hydrostatic pressure

TABLE I: The terms $\mathbf{S}_n h_1$ and their physical interpretation (terms 1-7 are identical to those in Ref. 5. $\tilde{f}_{hh}$ stands for f_{hh} without the contribution of the hydrostatic pressure.

Term	front mode	back mode	front mode (front only)	back mode (back only)
1	none	none	none	none
2	**stabilizing**	**destabilizing**	**stabilizing**	**stabilizing**
3	stabilizing	stabilizing	stabilizing	stabilizing
4	destabilizing	stabilizing	destabilizing	stabilizing
5	stabilizing	destabilizing	destabilizing	stabilizing
6	stabilizing	destabilizing	stabilizing	stabilizing
7	stabilizing	stabilizing	stabilizing	stabilizing
8	**destabilizing**	**stabilizing**	**destabilizing**	**destabilizing**
9	stabilizing	destabilizing	stabilizing	stabilizing
10	destabilizing	destabilizing	destabilizing	destabilizing
11	stabilizing	stabilizing	stabilizing	stabilizing

TABLE II: Effect of the terms $\mathbf{S}_n h_1$ on the stability of moving contact lines. The respective main stabilizing and destabilizing influences are marked by bold letters.

FIG. 1: Ridge profiles $h_0(x)$ for different values of the mean film thickness $\bar{h}$ (see legend) for $G = 10^{-5}$, $\alpha = 0.2$, $L = 20000$ and $a = 0.1$. The ridge is sliding towards the right.

FIG. 2: Transverse stability of a ridge on a horizontal substrate: (a) Ridge profiles $h_0(x)$ for different values of the mean film thickness as given in the legend. (b) Dispersion relation $\beta(k)$ for the two transverse modes when $\bar{h} = 1$: the unstable varicose mode (solid) and the stable zigzag mode (dashed). The corresponding modes are sketched in the inset. (c) The eigenmodes $h_1(x)$ corresponding to (b). The neutral modes obtained at $k = 0$ are indistinguishable from the modes for the other k in (b). (d) Dependence of the maximum growth rate β_{max} (left scale) and the corresponding transverse wavenumber k_{max} (right scale) on the mean film thickness $\bar{h}$. The remaining parameters are $\alpha = 0$, $G = 0.1$, and $a = 0.1$.

FIG. 3: Stationary profiles $h_0(x)$ (upper plots) and the corresponding eigenfunctions $h_1(x)$ (lower plots) for $k = 0$ (dotted line), at the maximum of the dispersion relation (Fig. 4) for small k (dashed line) and at the maximum for larger k (solid line, (b-d) only) when $\bar{h} = 1.5$ and (a) $L = 75$, (b) $L = 150$, (c) $L = 200$ and (d) $L = 500$. For narrow ridges the small k (large k) maximum corresponds to a zigzag (varicose) mode. For broader ridges the small k (large k) instability is localized at the front (back) of the ridge. The remaining parameters are $\alpha = 0.2$, $G = 0.1$, and $a = 0.1$.

FIG. 4: Dispersion relations $\beta(k)$ for $\bar{h} = 1.5$ and (a) $L = 75$, (b) $L = 150$, (c) $L = 200$ and (d) $L = 500$. Identical dispersion relations are obtained for $L = 500$ and (a) $\bar{h} = 0.59$, (b) $\bar{h} = 0.77$, (c) $\bar{h} = 0.88$ and (d) $\bar{h} = 1.5$. For $L < 75$ (at $\bar{h} = 1.5$) the results from these two approaches start to differ because the ridges in the different periods interact. The remaining parameters are $\alpha = 0.2$, $G = 0.1$, and $a = 0.1$. Thick (thin) lines indicate real (complex) modes.

FIG. 5: The maximum growth rate β_{max} at the two maxima of the dispersion relation as a function of the longitudinal period L. Parameters are as in Fig. 4 at fixed $\bar{h} = 1.5$.

FIG. 6: The linear stability results as a function of the longitudinal period L. The dashed lines show the critical wavenumbers k_c of the first two eigenvalues of the two modes (the small k mode in the upper left part of the plot and the large k mode in the upper right part). The system is linearly stable above the thick dashed and dotted lines (shaded region). The dashed line denotes the zero crossing of a real eigenvalue while the dotted line denotes the zero crossing of the real part of a complex eigenvalue. The complex mode exists in the parameter range enclosed by the thin dotted lines. The solid lines represent the transverse wavenumbers corresponding to local maxima in the growth rate, with the thick lines representing the absolute maximum. Parameters are as in Fig. 4 at fixed $\bar{h} = 1.5$.

FIG. 7: Stationary profiles $h_0(x)$ (upper plots) and corresponding eigenfunctions $h_1(x)$ (lower plots) for $k = 0$ (dotted line), at the maximum of the dispersion relation (Fig. 8) for small k (dashed line) and at the maximum for larger k (solid line, (b-d) only) when $L = 500$, $\bar{h} = 1.5$, $G = 0.1$, $a = 0.1$ and (a) $\alpha = 0.025$, (b) $\alpha = 0.05$, (c) $\alpha = 0.1$ and (d) $\alpha = 0.2$.

FIG. 8: Dispersion relations for (a) $\alpha = 0.025$, (b) $\alpha = 0.05$, (c) $\alpha = 0.1$, (d) $\alpha = 0.2$ and $L = 500$, $\bar{h} = 1.5$, $G = 0.1$ and $a = 0.1$. Thick (thin) lines indicate real (complex) modes.

FIG. 9: Maximum growth rate β_{max} as a function of the inclination angle α when $L = 500$, $G = 0.1$, $\bar{h} = 1.5$ and $a = 0.1$. Solid (dashed) lines indicate back (front) modes corresponding to the two local maxima of the dispersion relation at large k.

FIG. 10: As for Fig. 6 but showing the α dependence of the linear stability results for $L = 500$, $G = 0.1$, $\bar{h} = 1.5$ and $a = 0.1$.

FIG. 11: The maximum or minimum values h_{1m} of the eigenfunctions $h_1(x)$ at the front (dashed lines) and back (solid lines) of the ridge. The two different eigenmodes are indicated by heavy and thin lines. The dotted vertical lines indicate the values of k_{max} at the local maxima of the dispersion relation. The filled circles indicate the corresponding mode. The inclination angles α and other parameters are as in Fig. 8.

FIG. 12: The contributions β_n to the overall growth rate β of (a) the front and (b) the back mode, relative to their values at $k = 0$, plotted as a function of the transverse wavenumber k. The parameters are as in Fig. 4 (d) and the numbering follows Table I.

FIG. 13: The contributions of the front part, β^f, and back part, β^b, to the eigenvalue β for (a) the front mode and (b) the back mode. The parameters are as in Fig. 4 (d).

FIG. 14: The contributions β_n^b to the eigenvalue of the back mode. Normalization, term numbering and parameters are as in Fig. 12.

FIG. 15: Comparison of the full dispersion relation (heavy lines) with the small k dispersion relation derived in Sect. IV D (thin lines) for different values of L (given in the legend). The parameters are as in Fig. 4.

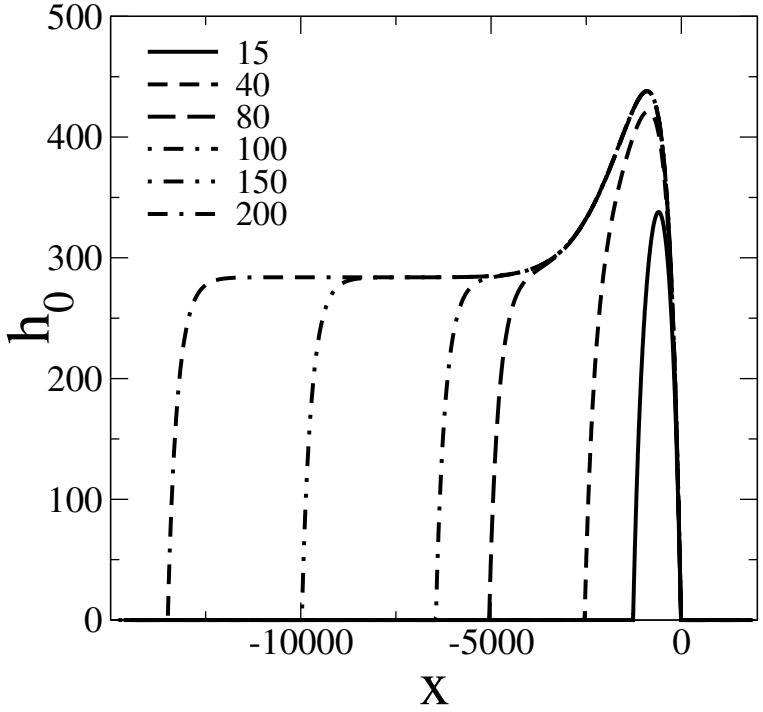

FIG. 1
Thiele, Phys. Fluids

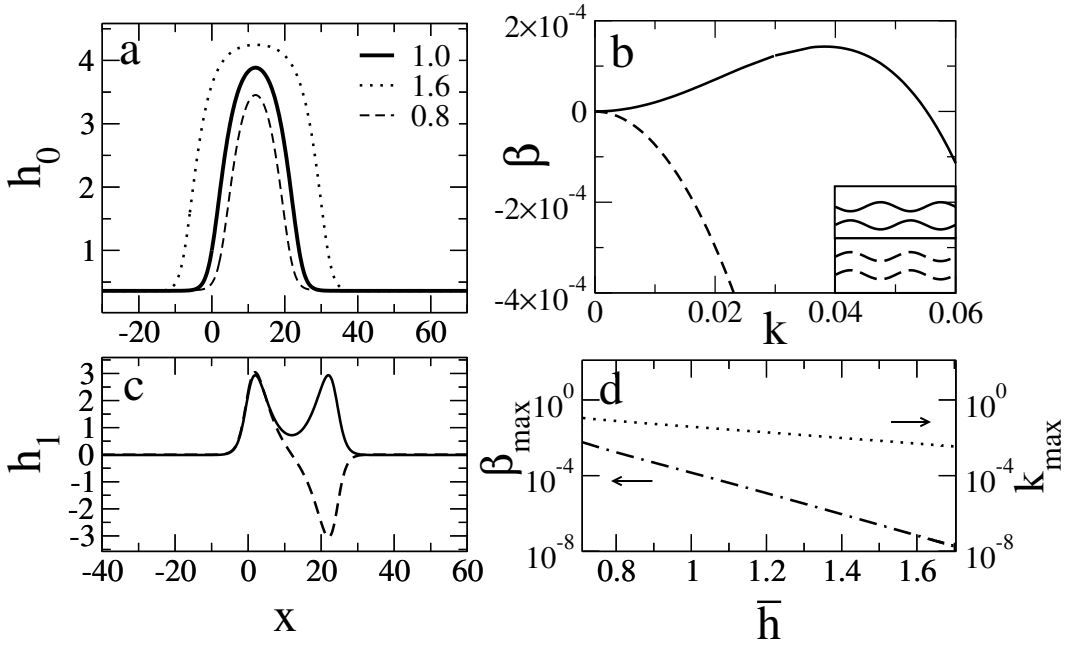

FIG. 2
Thiele, Phys. Fluids

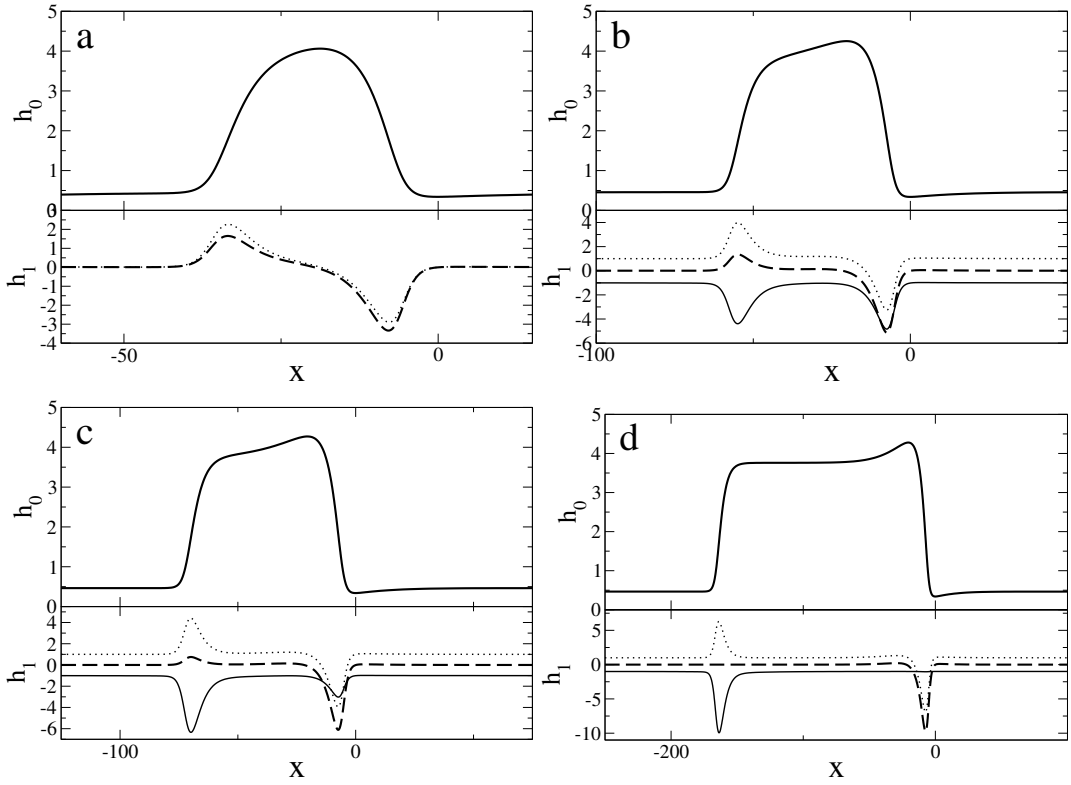

FIG. 3
Thiele, Phys. Fluids

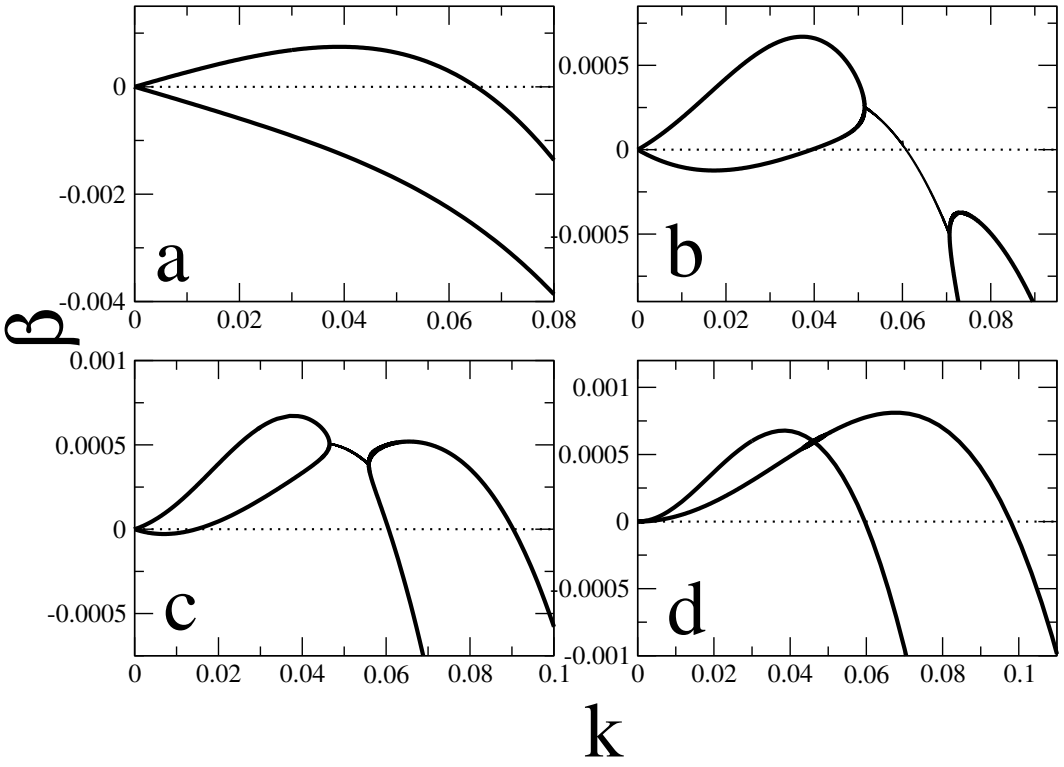

FIG. 4
Thiele, Phys. Fluids

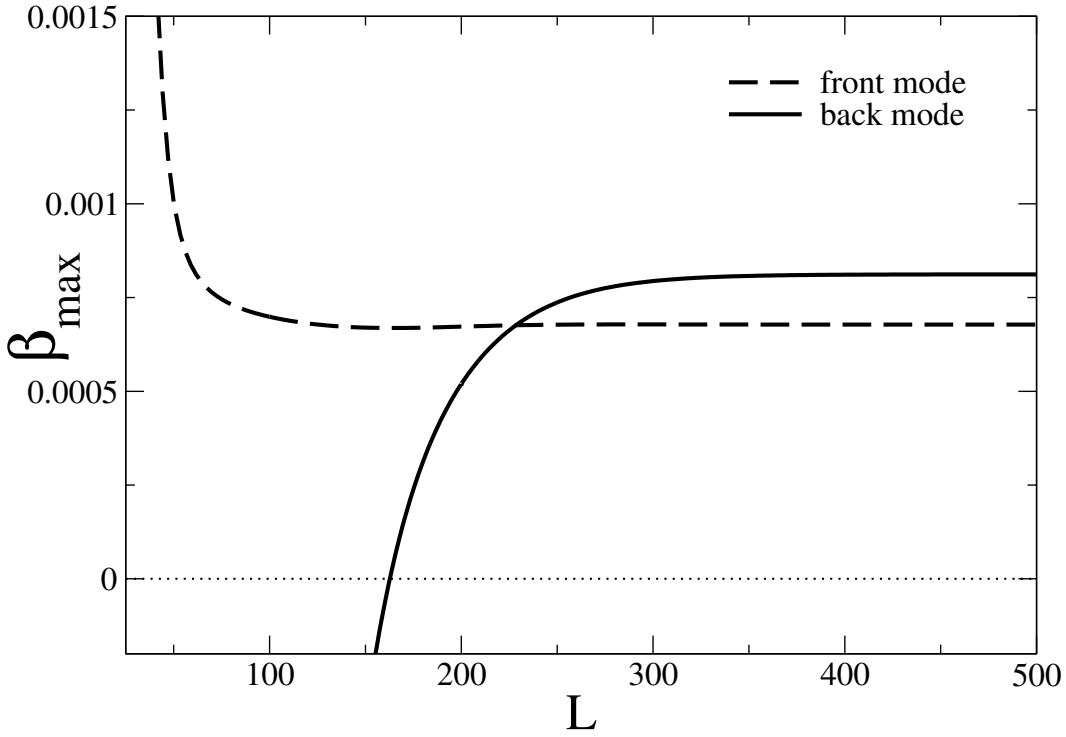

FIG. 5
Thiele, Phys. Fluids

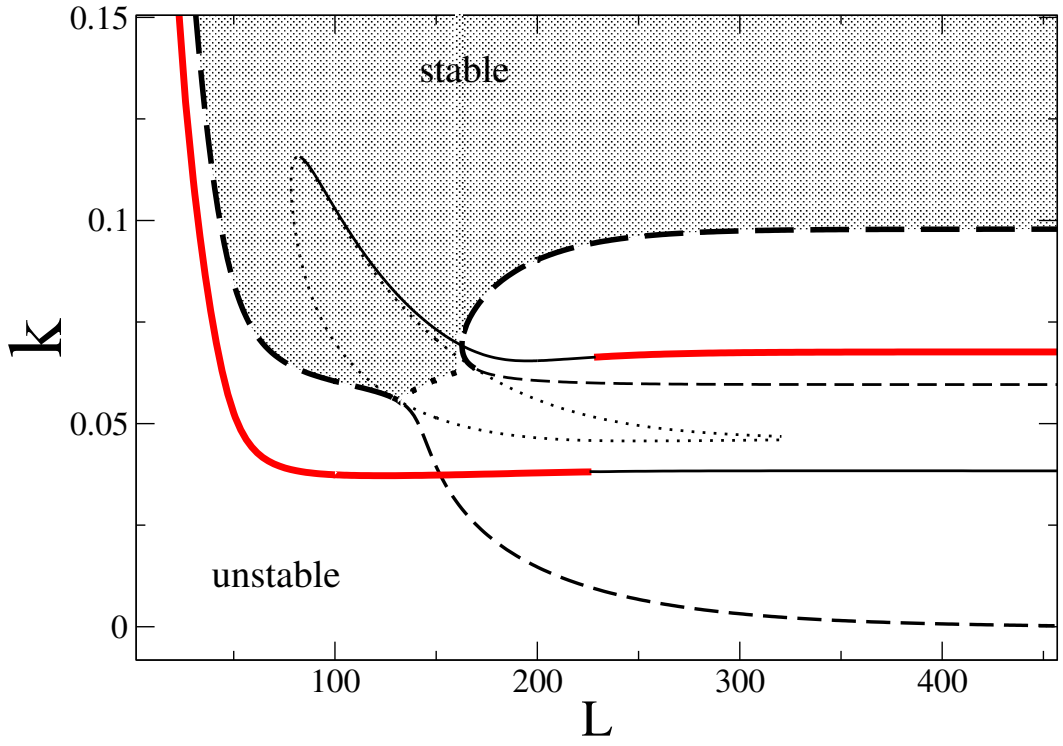

FIG. 6
Thiele, Phys. Fluids

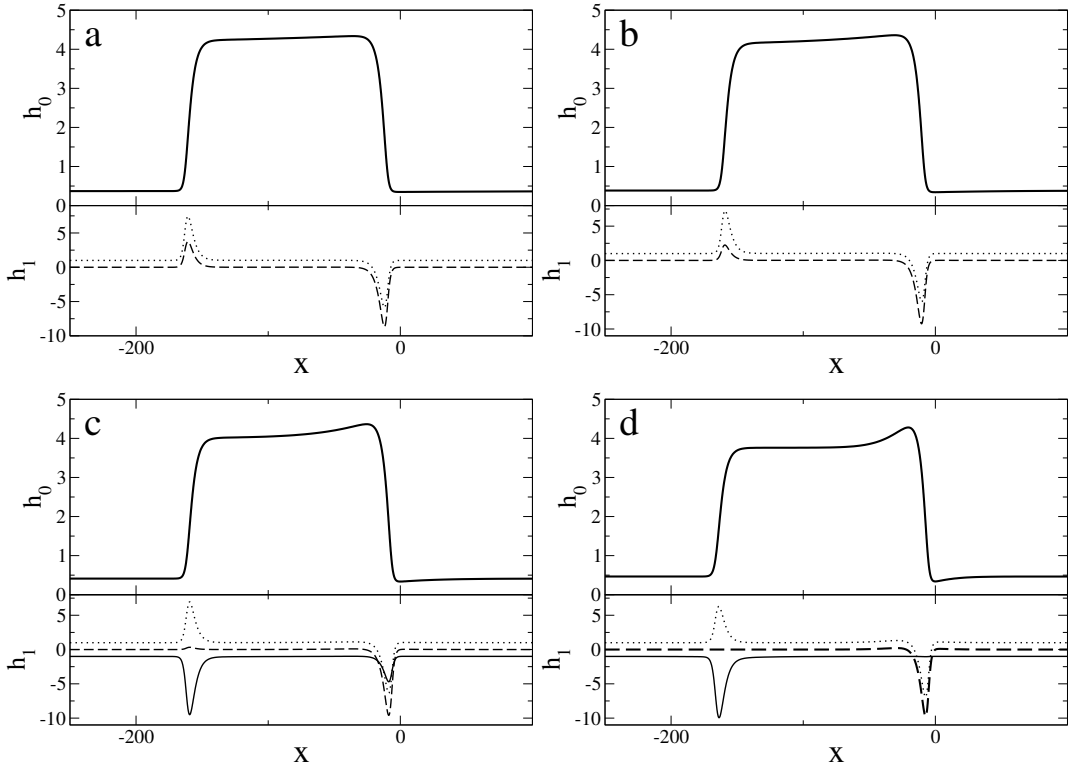

FIG. 7
Thiele, Phys. Fluids

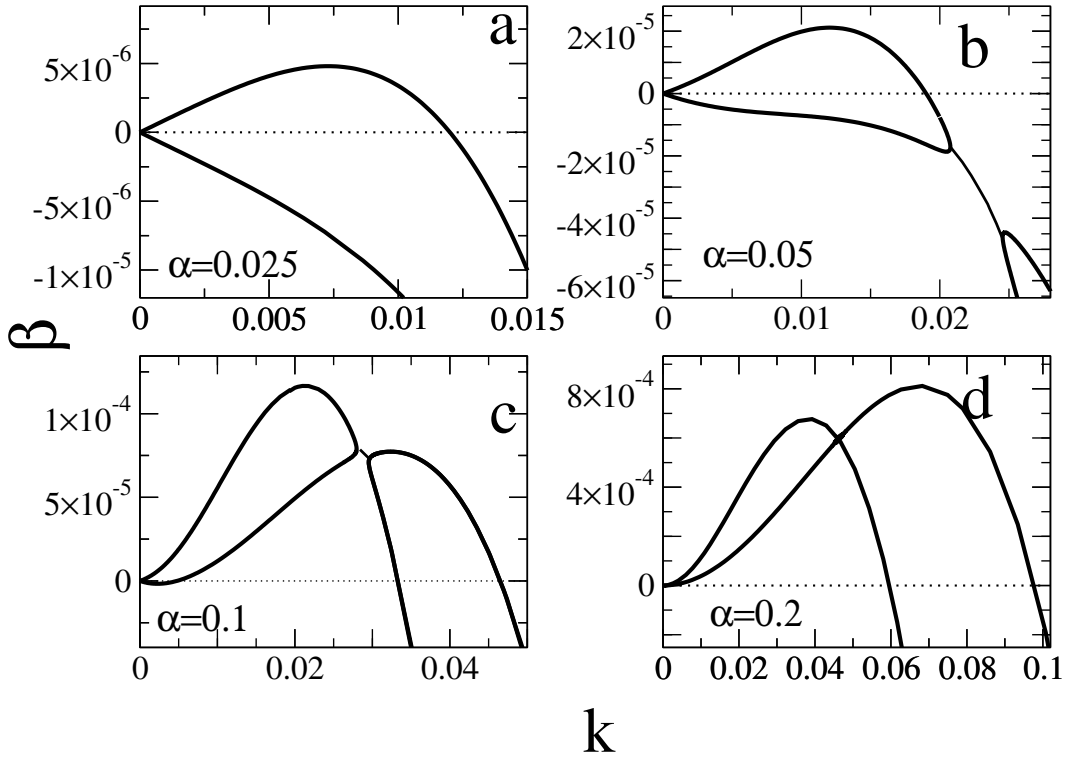

FIG. 8
Thiele, Phys. Fluids

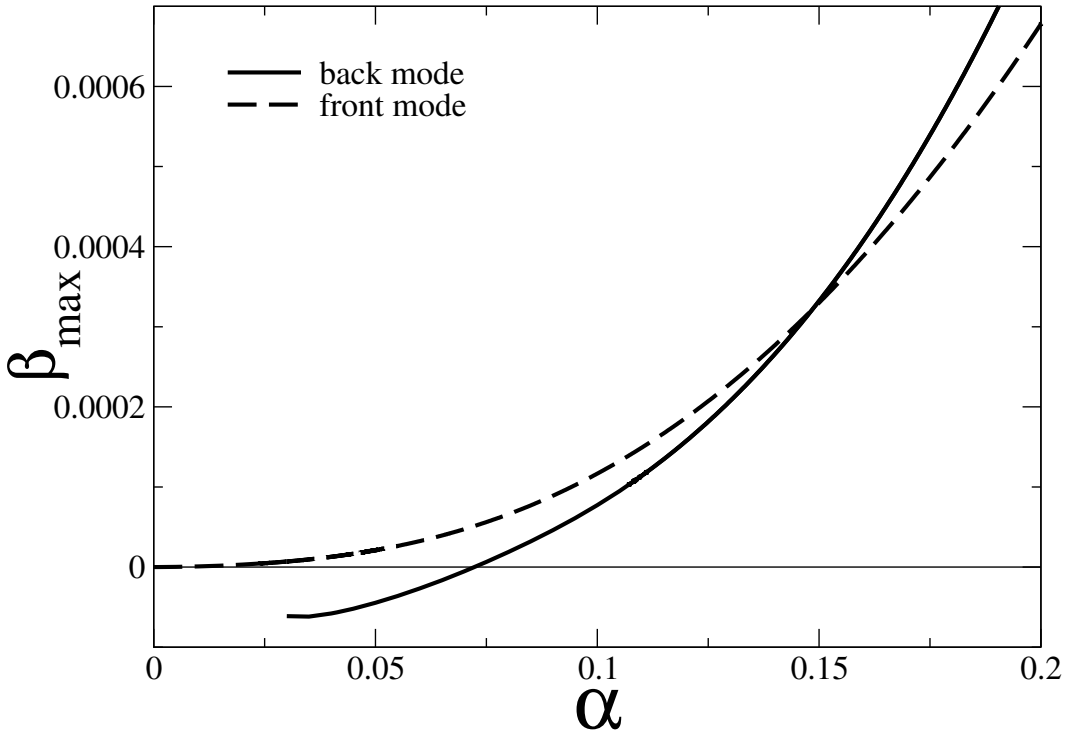

FIG. 9
Thiele, Phys. Fluids

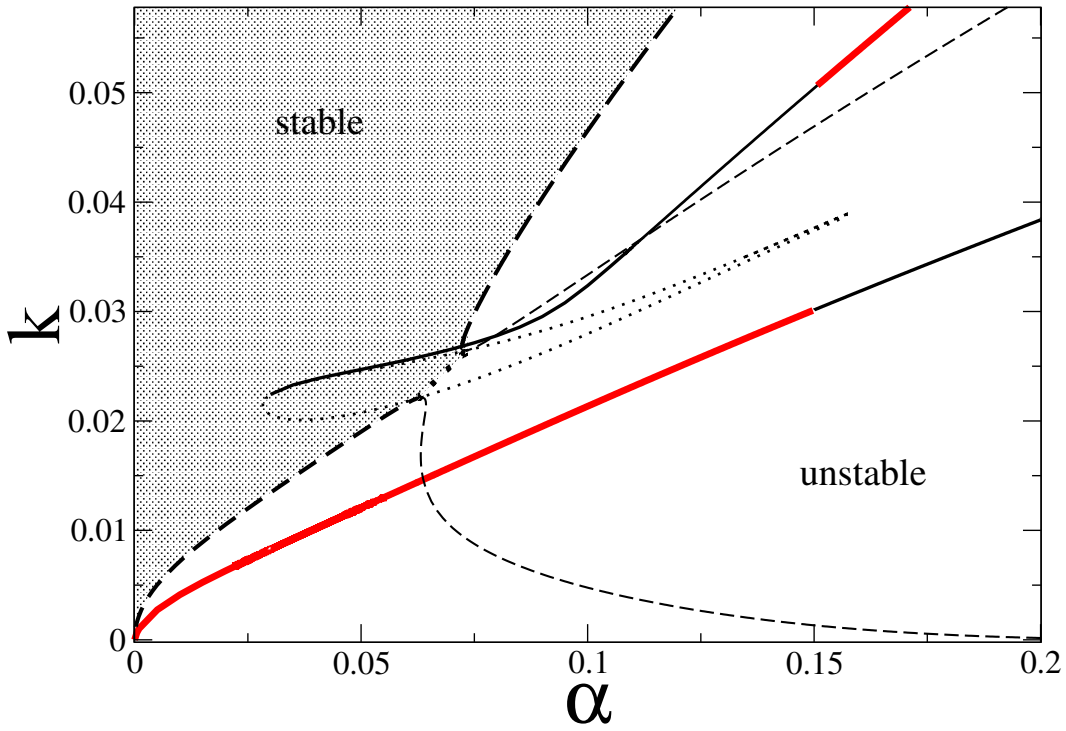

FIG. 10
Thiele, Phys. Fluids

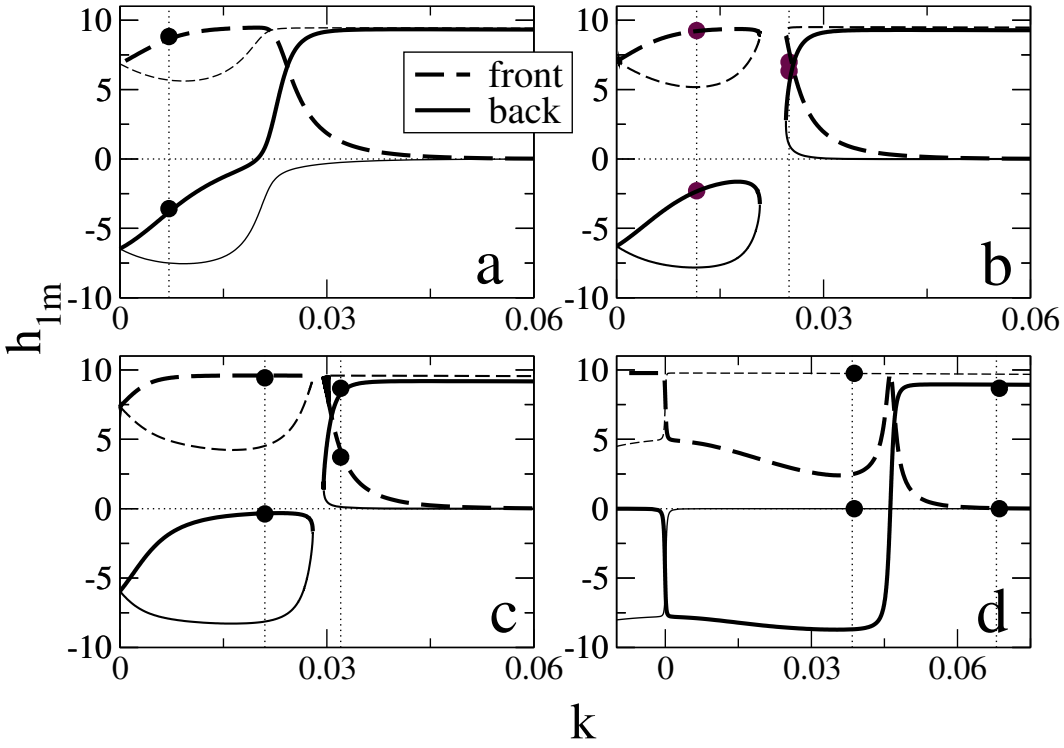

FIG. 11
Thiele, Phys. Fluids

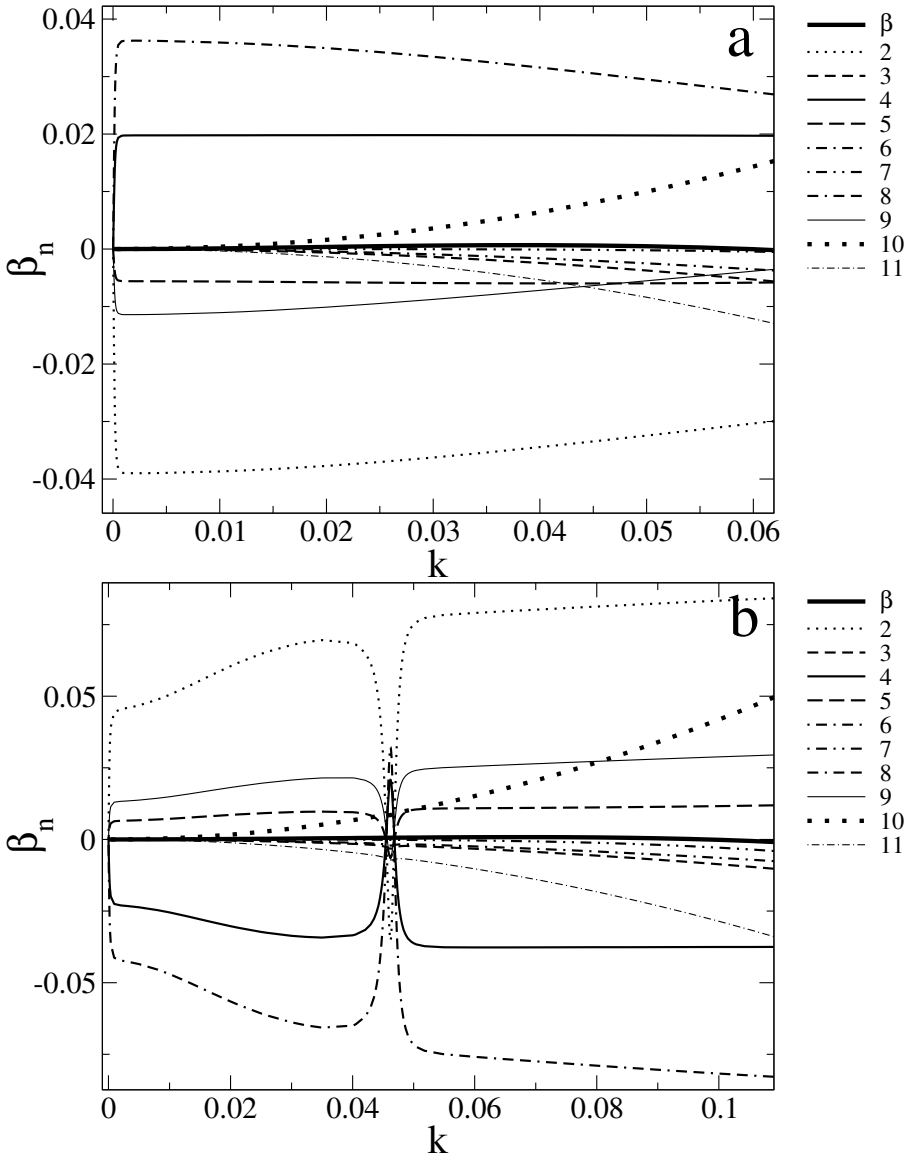

FIG. 12
Thiele, Phys. Fluids

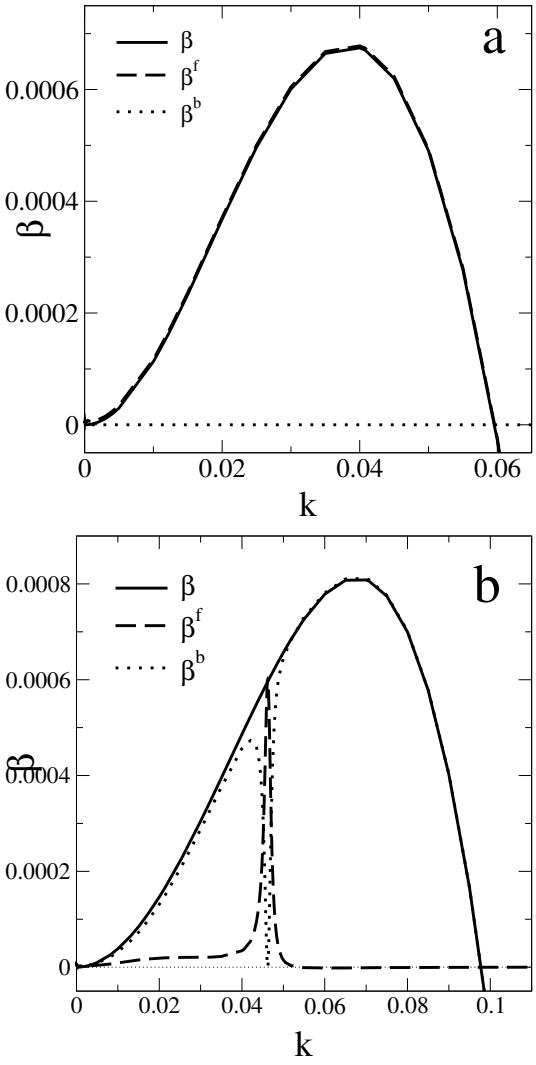

FIG. 13
Thiele, Phys. Fluids

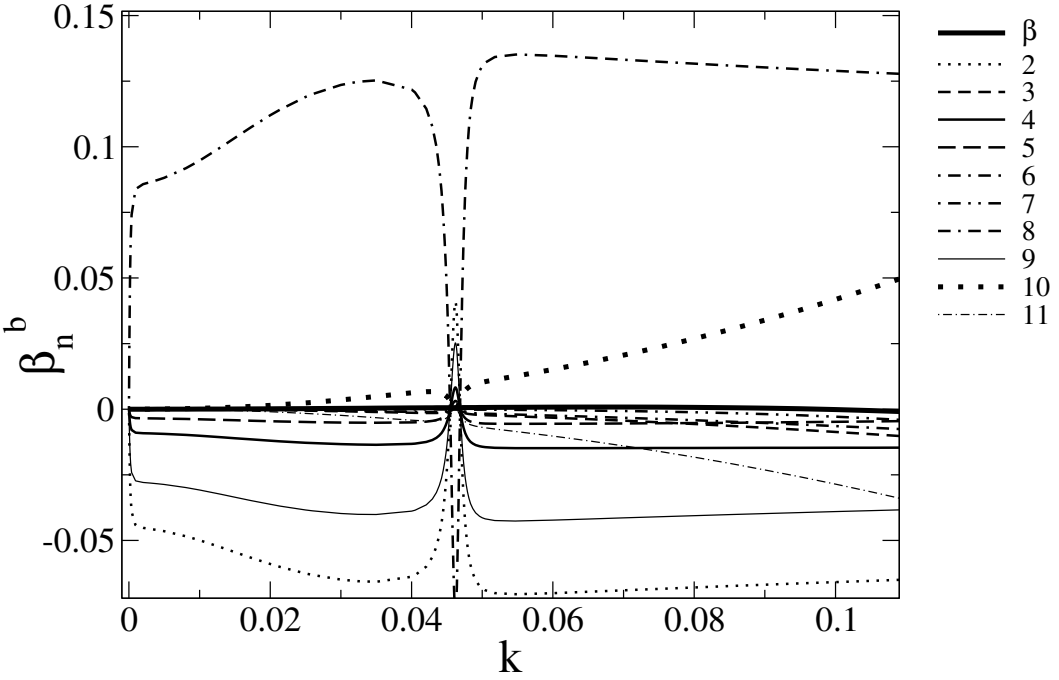

FIG. 14
Thiele, Phys. Fluids

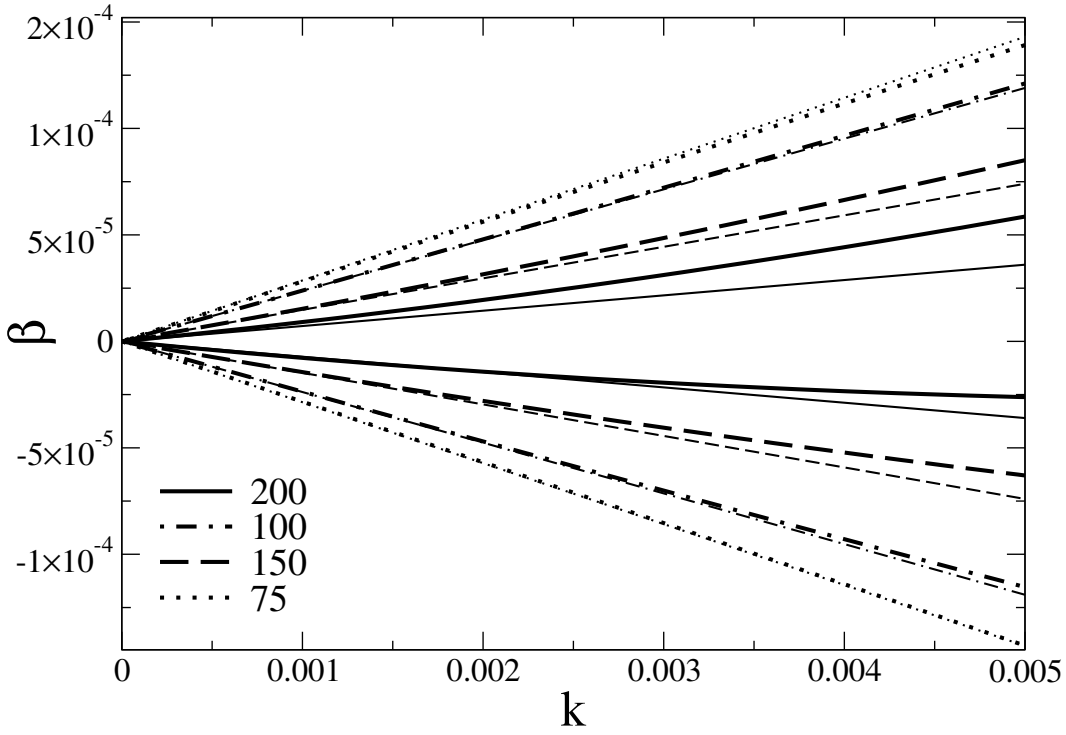

FIG. 15
Thiele, Phys. Fluids